THE JOURNAL OF PHYSICAL CHEMISTRY B

Feature Article

Cite This: J. Phys. Chem. B 2019, 123, 9507−9524

pubs.acs.org/JPCB

Energy Transport across Interfaces in Biomolecular Systems

David M. Leitner,* Hari Datt Pandey,† and Korey M. Reid

Department of Chemistry, University of Nevada, Reno, Nevada 89557, United States

ABSTRACT: Energy transport during chemical reactions or following photoexcitation in systems of biological molecules is mediated by numerous interfaces that separate chemical groups and molecules. Describing and predicting energy transport has been complicated by the inhomogeneous environment through which it occurs, and general rules are still lacking. We discuss recent work on identification of networks for vibrational energy transport in biomolecules and their environment, with focus on the nature of energy transfer across interfaces. Energy transport is influenced both by structure of the biomolecular system as well as by equilibrium fluctuations of nonbonded contacts between chemical groups, biomolecules, and water along the network. We also discuss recent theoretical and computational work on the related topic of thermal transport through molecular interfaces, with focus on systems important in biology as well as relevant experimental studies.

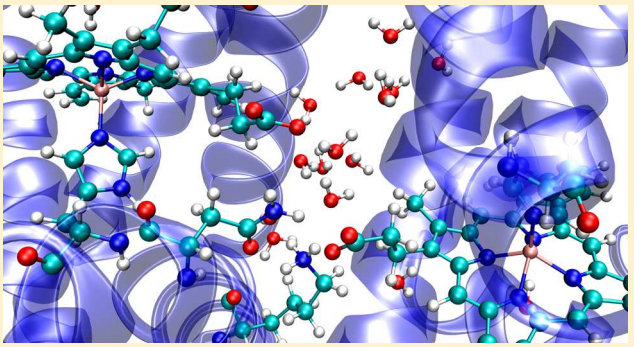

1. INTRODUCTION

Energy transport in biomolecules during chemical reactions in the cell occurs not only through the backbone of, say, a protein where the transformation takes place but also across myriad interfaces within the protein and between it and its surroundings. Time-resolved measurements and molecular simulations continue to provide an ever more detailed picture of energy relaxation during reactions and following photoexcitation in biological molecules,[1−23] mapping not only relaxation pathways and their role in subsequent reactions and cooperativity but also contributions of structure and equilibrium dynamics that control energy relaxation. In this Feature Article, we discuss recent work on energy transport through systems of biological molecules on sub-nanosecond time scales with focus on energy transfer across interfaces between chemical groups of large biomolecules and their surroundings. Statistical properties of energy transport in proteins on vibrational time scales have been analyzed,[1] and computational studies have long been elucidating pathways in specific proteins by which energy transport occurs, providing important insights into time-resolved measurements.[24−28] More recently, attention has turned to identifying rules by which structure and equilibrium fluctuations control energy transport, and we discuss that aspect here. We furthermore address recent work on the related topic of thermal transport in biological systems and systems with application to biological processes in the cell, also governed by vibrational energy transport through molecular interfaces. We discuss thermal conduction of interfaces between protein and water, protein−saccharide−water interfaces, and interfaces between water and gold nanoparticles functionalized for photothermal applications in cells.

A protein may be in a large number of structures in its functional state, as dictated by its energy landscape.[29,30] Over the vibrational time scales for energy transport that we address, the protein and its surroundings have little time for excursions beyond a local minimum or a few minima of that landscape. Because of structural aperiodicity, the vibrational dynamics of a protein and energy transport resemble to some extent those of glassy materials.[31−34] The statistical properties of energy transport on vibrational time scales have been well studied and reviewed in the past.[1] They are related to the mass distribution governed by protein geometry and by the vibrational dynamics associated with that geometry, as will be briefly summarized below. On a more microscopic level, we wish to identify rules by which specific contacts and their dynamics mediate energy transport. For instance, the rate of energy transfer across a nonbonded contact is often controlled not only by the chemical nature of the contact and distance between chemical groups but also by equilibrium structural fluctuations and energy relaxation within chemical groups of the system.[35−37] Connections between equilibrium dynamics and energy transfer not only help in modeling energy transport but can also provide a more detailed molecular-level picture underlying results of ongoing time-resolved spectroscopic experiments.

Energy transport in many biological molecules such as proteins differs from the more isotropic transport in many condensed phase systems in that the mass density of the medium is highly inhomogeneous. The mass distribution for several proteins is illustrated in Figure 1 and discussed further below. On length scales from about 2 Å to several nm, proteins exhibit properties of fractal objects, which provide a statistical

Received: July 24, 2019
Revised: September 8, 2019
Published: September 11, 2019

DOI: 10.1021/acs.jpcb.9b07086
J. Phys. Chem. B 2019, 123, 9507−9524

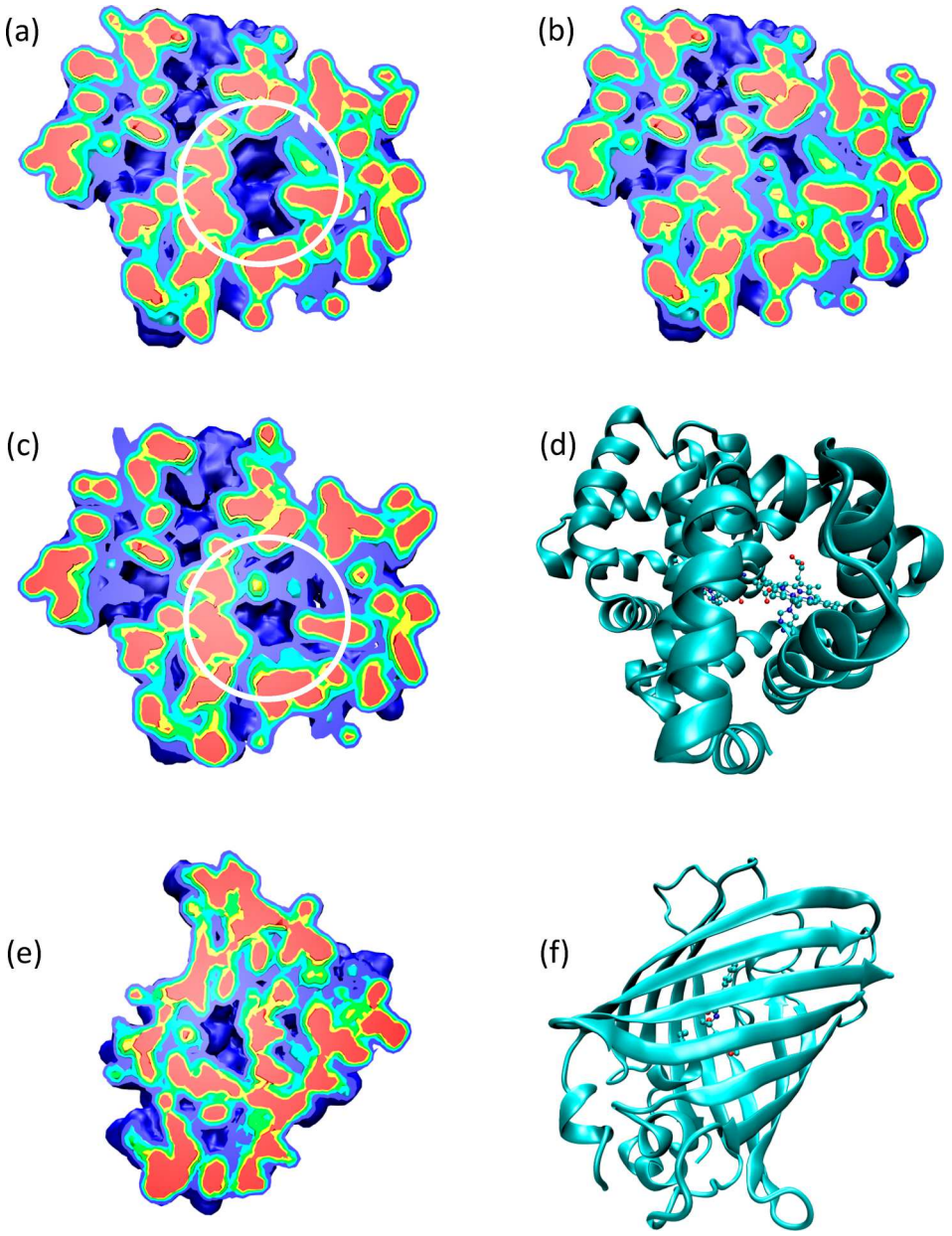

Figure 1. Density plots of deoxy-HbI with no (a) and with (b) water at the interface between the two globules. The interface region is circled in part a. (c) Oxy-HbI without the interface waters is shown with the interface region circled. A perspective for HbI (deoxy; oxy is nearly identical) is shown in part d. (e) A density plot of GFP using the perspective shown in part f. Each density plot is a slice through about the middle of the protein from the perspective that is indicated by the ribbon diagrams. Volume mass-density maps were created using a voxel size of 1.728 Å^3, which corresponds to a cube with sides of length 1.2 Å. The mass density is displayed in five levels which correspond to regions with a density of 0.116 amu/Å^3 (blue), 0.231 amu/Å^3 (cyan), 0.347 amu/Å^3 (green), 0.463 amu/Å^3 (yellow), and at least 0.579 amu/Å^3 (red), a region in which the density rises steeply. Networks of higher density through each protein are apparent. The interface region of oxy-HbI is smaller and holds less water than deoxy-HbI. Water is seen to enhance density in the interface (compare parts a and b) in HbI in both unliganded and liganded states.

description of energy transport and the emergence of networks of energy transport channels that span these molecules.[38−46] The statistical similarity between the distribution of mass on the level of amino acids and at larger length scales of groups of amino acids has been associated with the subdiffusive energy dynamics observed in computational studies,[38] vibrational dynamics of proteins,[47−49] and the anisotropy of energy transfer observed in time-resolved vibrational spectroscopy.[50,51] Statistical properties of mass distribution indicate that energy transport is anisotropic and networks for long-range energy transport are ubiquitous in globular proteins. Networks of energy transport in proteins and between protein molecules, including long-range nonbonded networks in allosteric proteins that also include water molecules,[52,53] have been identified by computational studies[15,53−67] and probed by experiment.[3,50,51,68−71]

To simplify the description of energy transport through a system of biomolecules, we consider first a coarse-grained picture of a protein and its environment. Though there are significant limitations to a Markov approximation in a model for energy transport in biomolecules, as long-wavelength modes make significant contributions,[72,73] master equation simulations appear to model the transport quite well when compared with results of all-atom nonequilibrium simulations,[35,37] as we summarize here. For such a simple model to be predictive, we

DOI: 10.1021/acs.jpcb.9b07086
J. Phys. Chem. B 2019, 123, 9507−9524

need an approach to estimate rate constants. We can broadly classify rate constants in two groups, one for energy transfer along the main chain and another for the more variable set of rate constants for nonbonded contacts. The former group has been quantified by experiments on helical peptides and by simulation for some time.[6,35,74−78] More recently, energy transfer across nonbonded contacts and properties that govern rate constants for that process have been analyzed.[35,36] For residue−residue and residue−water contacts, the rate of energy transfer has in some cases been found to vary inversely with fluctuations in the length of the contact.[35,36] Such a relation can help determine rate constants for a master equation from relatively short equilibrium simulations of proteins.

Thermal transport across interfaces is mediated by vibrational dynamics and energy relaxation. We discuss studies of thermal transport across protein−water interfaces,[57,79−81] which may include layers of other molecules such as saccharides,[82] to provide a general picture of thermal transport through interfaces in biological systems and its role in heat flow in the crowded environment of the cell.[83−85] We also discuss other recent work[86−89] on contributions of molecular structure, composition, and energy relaxation and thermalization in thermal transport across molecular interfaces, in which a vibrational state space picture of energy flow in molecules,[90−100] developed to describe quantum energy flow in modest-sized molecules and its role in chemical reaction kinetics, can be helpful. We focus on systems in a cellular environment, including thermal transport between a gold nanoparticle (GNP) and its surroundings via a capping agent that functionalizes the GNP for photothermal applications,[101−104] such as drug delivery and control of protein and nucleic acid structure and aggregation.

This Feature Article is organized into two parts. The first addresses energy transport in systems of biomolecules, with focus on energy transfer across nonbonded contacts. In section 2, we provide some background to energy transport in proteins, its relation to protein geometry, and attempts to use Markov models to describe energy transport. In section 3, we discuss relations between biomolecule structure, equilibrium structural fluctuations, and energy transfer. A central topic is the relation between equilibrium structural fluctuations and energy transfer across contacts between amino acids, cofactors, and water. In the second part of the article, we address thermal transport across molecular interfaces. In section 4, we consider thermal transport across protein−water interfaces and how thermal conductance of the protein−water interface changes with a layer of saccharides on the protein surface. In section 5, we turn to a more general discussion of thermal conductance of molecular interfaces between two larger objects, which could be protein and water, or a gold nanoparticle and the cellular environment. Section 6 presents a summary and future directions.

2. ENERGY TRANSPORT IN PROTEINS AND PROTEIN GEOMETRY

We summarize here some important properties that control energy transport within proteins and interfaces with other biomolecules. Within a protein, there are numerous interfaces and gaps between residues, giving rise to a highly nonuniform mass density, as long recognized.[105] Before summarizing the connection to energy transport, we illustrate heterogeneous mass density with several examples in Figure 1, where we depict slices through proteins from the perspective illustrated by the accompanying ribbon diagram.

The proteins plotted include the homodimeric hemoglobin from *Scapharca inaequivalvis* (HbI), both in liganded and unliganded states. To contrast with a helical protein, we also show the β-barrel green fluorescent protein (GFP). Regardless of structural makeup, globular proteins are characterized by networks of high density and many low-density pockets. Some of those low-density regions contain water molecules, including parts of the interior of GFP and the interface between the two globules of HbI. The latter is indicated with a circle in the density plots. There are more water molecules at the interface of HbI in the unliganded state, corresponding to a larger low-density region when the mass density plot does not include the interface water. The density plots with the interface water present clearly reveal a higher density at the interface than when the water is absent. Of course, what molecules are embedded in regions of low protein density depends on the chemical composition of the region. Overall, the density plots for the proteins reveal more the organization of the amino acid residues than the structure of the backbone, which tethers the amino acids together. It is the structure as revealed by the mass density as well as fluctuations in that structure that control energy transport and signaling. Once again, we picture the protein and water in a local minimum of a complex energy landscape, where it resides on time scales of vibrational energy transport. Fluctuations in structure thereby correspond to oscillations of contacts within that local minimum.

In connecting energy transfer in a protein to the heterogeneity of mass density, we begin with a statistical perspective.[1] Over length scales from a few atoms to the size of the protein, about 2 Å to several nm in length, the mass density can be described by fractal geometry, where the mass, M, of amino acids contained inside a sphere of radius R is found to scale with R as $M \propto R^D$, where D is referred to as the mass fractal dimension. D is less than 3 for folded proteins, reflecting the heterogeneity of the density in the protein interior. For the inner region of a protein, the mass fractal dimension approaches a value of roughly 2.6 for larger proteins and may be smaller for smaller proteins.[39,40] A dimension of 2.6 is similar to the dimension of a percolation cluster near threshold in three-dimensional space, the point at which channels connecting one region of the surface to any other is guaranteed, even if there are many pockets in the interior where there are few contacts, restricting energy transport there. Due to the fractal nature of the protein interior, the mass distribution on a small scale, such as a few atoms, looks statistically similar to that on a larger scale, such as clusters of residues.[44] The observation that $M \propto R^D$, where $D \approx 2.6$, helps to explain energy transport in proteins.

The inhomogeneous distribution of mass in a protein is correlated with anisotropic energy transport. Molecular simulations of energy transport through proteins on the vibrational time scale find a correlation between facile transport and regions of high density, which can span a protein molecule, as the percolation picture suggests.[38] One striking example has been discussed in the simulations of protein quakes in myoglobin, which revealed a propensity for energy transport through the high-density regions following ligand photolysis, ultimately yielding pressure waves in the surrounding solvent.[66] Correlations between high mass density and energy transport have also been observed in time-resolved X-ray studies of HbI following ligand photolysis, which reveal events involved in allosteric transitions from the liganded to unliganded state.[20,106,107] These results are consistent with a mass density

DOI: 10.1021/acs.jpcb.9b07086
J. Phys. Chem. B 2019, 123, 9507−9524

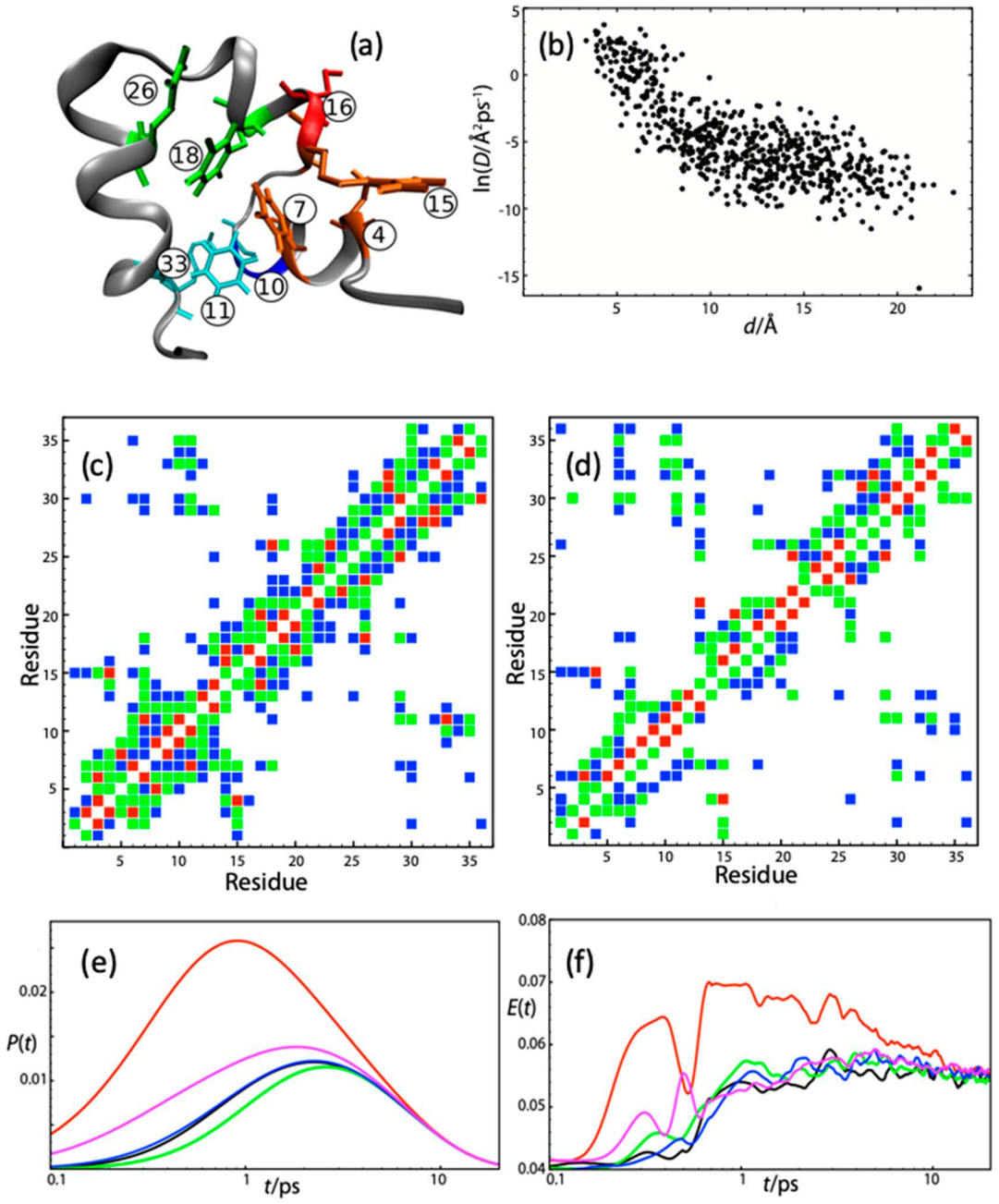

Figure 2. (a) Villin headpiece subdomain (HP36) with some of the residues discussed in text highlighted. (b) Natural log of local energy diffusivity, $\ln(D_{AA'})$, vs inter-residue distance, d, for HP36. $\ln(D)$ typically decreases with increasing d, though there are significant fluctuations around this trend. Larger $\ln(D_{AA'})$ values at a corresponding d typically correspond to charged residues, whereas smaller values correspond to nonpolar residues. (c) Distance map, residue pairs for which distance, $d < 5$ Å (red), 7 Å (green), and 9 Å (blue). (d) Communication map: $D_{AA'} > 10$ Å^2/ps (red), 1 Å^2/ps (green), and 0.1 Å^2/ps (blue). The lower triangle in parts c and d corresponds to the dehydrated structure, and the upper triangle corresponds to hydrated HP36. (e) Master equation simulation of $P(t)$ using for rate constants the data in part d. (f) All-atom nonequilibrium MD simulation of kinetic energy per degree of freedom, $E(t)$, for residues 3 (black), 4 (red), 5 (green), 6 (blue), and 7 (magenta) when residue 16 is heated initially. These results highlight the importance of the nonbonded contact between residues 4 and 15 in energy transport in HP36, as energy is transferred to residue 4 on a sub-ps time scale via the nonbonded contact, captured well by the master equation simulation without the statistical noise in the all-atom simulation. A phenomenological damping time of 5 ps is used for coupling to water in the master equation simulation, which appears to overestimate damping at the low temperature at which the all-atom simulation is run. There are no fitting parameters in the master equation simulations. When the rate constants of the master equation are obtained by fitting to results of all-atom simulations, the time-dependent energy in each residue predicted by the master equation simulation matches that of the all-atom simulations even better.[35] Reprinted with permission from ref 37. Copyright 2015 American Institute of Physics.

structure that in large part controls energy transport and signaling.

The anisotropic flow of energy in a protein and its dimension, D, can be related in a more quantitative fashion. We observed in computational studies of energy transport in proteins that, following a localized excitation, vibrational energy propagates subdiffusively; i.e, if $\langle R^2 \rangle$ is the variance in energy at time t, it spreads in a power law fashion as $\langle R^2 \rangle \propto t^{\alpha}$, where $\alpha < 1$.[38] The

DOI: 10.1021/acs.jpcb.9b07086
J. Phys. Chem. B 2019, 123, 9507−9524

power α depends both on the mass fractal dimension, D, which can be computed for objects such as those in Figure 1, as well as on a dynamic property, the spectral dimension, $\bar{d}$, which describes how the vibrational density of states, $\rho(\omega)$, varies with mode frequency, $\rho(\omega) \propto \omega^{\bar{d}-1}$. The subdiffusive transport of energy, with power $\alpha = \bar{d}/D$, thus depends on static and dynamic properties of the network.[1] In more recent work, we have moved beyond a statistical perspective of energy transport and explored specific properties of a protein that control energy transport and how measurements of energy transfer can inform us about protein structure and dynamics associated with energy transport and functionally important properties. These properties include not only the contacts that produce the structures and mass density plotted in Figure 1 but also equilibrium structural fluctuations of the protein.

We now seek to identify the networks along which energy transport occurs in a given biomolecular system. In a protein, such a network includes both the main chain and many interfaces, or nonbonded contacts, between residues. Network analysis of proteins is widely applied to identify groups of residues that interact, residues that are critical to communication, and regions where mutation might affect function.[43,108−122] Many definitions of networks are based on distance criteria, sometimes interactions, but our focus is on networks of energy transport channels. A natural computational approach to locate energy transport networks in proteins involves coarse-graining at the level of residues and perhaps clusters of water molecules. There are long-wavelength modes in proteins that play a role in energy transport.[31,38,72,73,123,124] Thus, coarse-graining at the level of residues and introducing a Markov model for energy transfer between them is a significant approximation. Nevertheless, we will explore the use of that picture. One assumption of the approach is sufficiently rapid energy relaxation within each residue, which is supported by calculations of anharmonic decay of vibrational states of proteins.[72] If we model transport with a master equation, we need to identify rate constants for energy transfer, both along the main chain and across nonbonded contacts.

We have developed an approach to locate energy transport networks by computing local energy diffusion coefficients, $D_{AA'}$, between residues A and A′.[15,53,56−58,79,125] In earlier work, we computed thermal transport coefficients of proteins,[72,126] a topic we have reviewed in the past,[1,127] and some of those values, which have been confirmed experimentally,[128] will be discussed in the following section. We note that both calculations and experiments of the thermal conductivity of proteins indicate enhancement of thermal transport due to anharmonic interactions, supporting a picture of fast energy relaxation that is assumed in the Markov model. On the basis of calculation of local contributions to the overall thermal diffusivity of a protein, we obtain energy diffusion coefficients $D_{AA'}$ between regions A and A′, which may represent residues, cofactors, or water. We have referred to the collection of values of $D_{AA'}$ for a particular protein or other nanoscale object as a communication map.[58]

We have computed and analyzed the local energy diffusion coefficients, $D_{AA'}$, between residue pairs for a number of proteins. For myoglobin, the energy transport networks that emerge from this calculation[58,129] have served as a good predictor for measurements of energy transport.[50,71] We have also compared energy transport predicted by a master equation simulation, where the rate constants are obtained in terms of $D_{AA'}$, with the results of all-atom nonequilibrium molecular simulations of energy flow in the same protein.[37] That study was carried out on the villin headpiece subdomain, HP36, which we summarize here. The protein is illustrated in Figure 2, indicating some of the residues that are important in energy transfer across nonbonded contacts. We also illustrated in Figure 2 the local energy diffusion coefficient, $D_{AA'}$, between A and A′ for HP36.

We observe in Figure 2 that values of $D_{AA'}$ are to some extent correlated with interresidue distance, d. However, they also depend on specific interactions between the residues. As seen in Figure 2b, there is great variability in the value of $D_{AA'}$ for a given distance, d, between the residues. For a given d, larger values of $D_{AA'}$ are found for interactions involving at least one charged residue, whereas smaller values of $D_{AA'}$ for a given d correspond to nonpolar pairs.[37] A distance map is plotted in Figure 2c, and a plot of the magnitude of $D_{AA'}$ for all residue pairs of HP36 is plotted in Figure 2d, both for the hydrated and dehydrated protein, i.e., communication maps for HP36. Comparing parts c and d of Figure 2, we see that, while the distance between two residues, A and A′, is often correlated with the local energy diffusivity, $D_{AA'}$, there are many cases where such a correlation appears weak. Due to nonbonded contacts, relatively large values of $D_{AA'}$ may be found for residues quite far from each other in sequence. For example, residues 4 and 15, which are hydrogen bonded, are seen to be close to each other and $D_{4,15}$ is relatively large; it is a similar case for nearby residues 11 and 33 and 18 and 26. Because of the relatively large values of the local energy diffusivity for these pairs, we might expect energy transfer through these contacts to compete with transport along the main chain, for which values of $D_{AA'}$ are comparable. Residues 3 and 15 are quite close to one another, but the local energy diffusivity between them is very small. Consequences of small $D_{3,15}$ and large $D_{4,15}$ are seen in the results of the master equation simulations.

The local energy diffusion coefficients may then be used to calculate rates of energy transfer between a residue pair. The rate constants, in turn, can be introduced into a master equation to model energy transport in a particular protein, or, more specifically, for a protein structure that may be one of many representing the native state. We thereby estimate a rate constant, $w_{AA'}$, for energy transfer between the residue pair A and A′ for a particular protein structure, assuming one-dimensional diffusion between them, so that the rate constant is $w_{AA'} = 2D_{AA'}/d^2$, where d is a representative distance between the residues. Those rate constants can then be introduced into a master equation of the form $dE_A/dt = \sum_{A' \neq A} w_{AA'}E_{A'} - w_{A'A}E_A$, where E_A is the energy of residue A and $w_{AA'}$ is a rate constant between residues A and A′. Different rate constants are in general needed if the protein samples other structures.

There are of course a number of assumptions in this master equation formulation. One is the Markov model assumption of memory loss at the scale of individual residues. That assumption ignores longer wavelength modes that span several residues and water, which is of course dynamically coupled to the protein.[130−139] While long wavelength modes transport vibrational energy in proteins, there are sufficiently many with wavelengths on the scale of individual residues and smaller that, even at low temperature, a Markov assumption yields results that apparently compare well with the results of all-atom simulations where comparison has been made.[37] In Figure 2e and f, we show results for solvated HP36, where the protein is initially cold and excited at residue 16. For the master equation results, we plot the

DOI: 10.1021/acs.jpcb.9b07086
J. Phys. Chem. B 2019, 123, 9507−9524

time-dependent probability for energy in a particular residue, while the time-dependent energy in a residue is plotted from the results of the all-atom simulations. To emphasize the role of nonbonded contacts in rapid energy flow in the protein, we focus on residues 3−7, far in sequence from the initially excited residue 16. Nevertheless, because of the large value of $D_{4,15}$ that results from the hydrogen bond between those residues, energy is transferred to residue 4 at times below 1 ps. Indeed, energy transfer to residue 4 following excitation at residue 16 occurs more rapidly than energy transfer to residue 14.

The time for energy transfer to residue 4, and subsequent transfer to nearby residues, is captured quantitatively by the master equation simulations, where the rate constants are obtained by the local energy diffusion coefficients in the communication map for this protein, and as noted above, we clearly see the consequences of large $D_{4,15}$ and small $D_{3,15}$ in the master equation results. To account for coupling of the protein to the surrounding water in the master equation simulation, a phenomenological damping rate was introduced. For solute modes in water, the damping rate can vary widely and we simply used a 5 ps lifetime as the representative for a protein in water, in rough agreement with results of experimental and computational studies of energy flow from peptides and proteins into water.[35,140] In the present case, where the all-atom simulations were run at low temperature (<100 K), the damping rate that was applied appears to be an overestimate. Overall, agreement between the master equation simulations and the results of the all-atom simulations is quite good given the simplicity of the approach to estimate rate constants and the Markov approximation at the level of individual residues. The importance of the nonbonded contact between residues 4 and 15 in energy transport is captured well by master equation simulations without the statistical noise in the all-atom simulation and without fitting parameters. When the rate constants of the master equation are fit to the results of the all-atom simulations, we find an even better match.[35] These studies provide insights into the origins of anisotropic energy transport from a relatively hot region to colder regions of the biomolecule and the solvent.

3. ENERGY TRANSFER RATES AND EQUILIBRIUM FLUCTUATIONS OF NONBONDED CONTACTS

We consider separately energy transport along the main chain and energy transfer across nonbonded contacts. The nature of energy transport along the main chain has been studied computationally and by time-resolved vibrational spectroscopy of helical peptides, which indicate diffusive energy transport along the peptide.[6,35,77,141,142] Results of all-atom nonequilibrium simulations of energy flow in HP36, discussed in the previous section, have been fit to a master equation, with rate constants for energy transfer along the main chain that are consistent with an energy diffusion coefficient, $D_{AA'}$, for neighboring residues that is on the order of 1 nm^2 ps^{-1}.[35] This value is similar in magnitude to values for many nonbonded contacts, and some rules governing energy transfer across nonbonded contacts have been identified by the HP36 study and more recent work.[35,36]

Energy transfer through nonbonded contacts competes with energy transfer between adjacent residues on the main chain, as illustrated by the computational results plotted in Figure 2 for HP36. That transfer depends on the proximity of residue pairs and the nature of the contact. Energy transfer across a hydrogen bond typically occurs more rapidly than that across a van der Waals contact. However, in both cases, the rate of energy transfer appears to depend on fluctuations in the length of the contact.

Before discussing some of the numerical evidence for the connection between energy transfer rates across nonbonded contacts and fluctuations in the contact length, we first summarize theoretical justification for such a connection. Consider a network as a collection of balls connected by springs, as in elastic models.[60,143−145] The equation of motion for the lattice vibrations is $m_A(d^2u_A/dt^2) = \sum_{A'\neq A} f_{AA'}u_{A'}$, where m_A and u_A are the mass and displacement, respectively, at site A and $f_{AA'}$ is the force constant for the interactions connecting the masses. This equation has the same form as a master equation, $dE_A/dt = \sum_{A'\neq A} w_{AA'}E_{A'} - w_{A'A}E_A$, for energy transfer between residues, where E_A is the energy of residue A and $w_{AA'}$ is a rate constant between residues A and A′. Both equations may include additional molecules such as solvent. We see that the equations differ by the presence of first- and second-order time-derivatives in the master equation and the equation of motion for lattice vibrations, respectively. As a result, some solutions to the master equation can be obtained from solutions to the vibrational dynamics by substituting t for ω^{-2}.[146−149]

For example, using the t to ω^{-2} (or reverse) substitution provides a connection between vibrational energy diffusion in a protein and its dispersion relation. The dispersion relation for a protein, describing how frequency, ω, varies with wavenumber, k, follows a power law relation, $\omega \propto k^a$,[38] as found for fractal objects.[149] Starting with this dispersion relation and using the ω^{-2} to t substitution, we find how the variance in energy in a protein spreads with time. The wavenumber, k, varies inversely with length, so that, rearranging $\omega \propto k^a$, length varies with frequency as $\omega^{-1/a}$. Following a localized excitation in a protein, vibrational energy, where $\langle R^2\rangle$ is the variance in the energy at time t, spreads in a power law fashion as, $\langle R^2\rangle \propto t^\alpha$.[38] Therefore, length varies with time as $t^{\alpha/2}$. Since t can be replaced by ω^{-2} in going from the solution of a diffusion equation to the vibrations of the object, we see that length varies as $\omega^{-\alpha}$. We already found that length varies as $\omega^{-1/a}$, so the two powers, a and α, are related by $a = \alpha^{-1}$. Calculations of dispersion relations and energy transport dynamics for specific proteins have yielded results where $a = \alpha^{-1}$. Calculation of the dispersion relation, $\omega \propto k^a$, for the proteins GFP and myoglobin yielded a = 1.56 and 1.69, respectively.[38] Vibrational energy dynamics determined by simulations yielded α = 0.64 and 0.58 for GFP and myoglobin, respectively,[38] consistent with $a = \alpha^{-1}$.

The same substitution allows us to connect energy transfer rates with equilibrium structural fluctuations. Consider the rate of energy transfer between two residues, A and A′. We drop the subscripts AA′ in the discussion that follows, recognizing that the rate constants and fluctuations in contact distance refer to a specific pair. We picture fluctuation in the distance of a contact, such as the length of a hydrogen bond, which may be a localized oscillation or may be an oscillation that is part of a delocalized mode or modes of the protein. Following the connection between time and frequency noted above, the rate constant, which varies as t^{-1}, can be replaced by ω^2. For an oscillator $\omega^2 \propto \langle\delta r^2\rangle^{-1}$, so that for a rate, $t^{-1} \propto \langle\delta r^2\rangle^{-1}$, or the rate constant varies as $w \propto \langle\delta r^2\rangle^{-1}$. While the vibrational model we have used to justify these relations is harmonic, we compare the trends that are predicted by it with the full anharmonic dynamics of the protein.

DOI: 10.1021/acs.jpcb.9b07086
J. Phys. Chem. B 2019, 123, 9507−9524

That the energy transfer rate across a nonbonded contact varies inversely with the variance in the length of the contact was first observed in the computational study of energy transport in HP36.[35] That study was carried out at low temperature, below 100 K, to increase signal-to-noise. For polar contacts, it was found that, for a given variance in contact distance, the energy transfer rate is greater than that for a nonpolar contact, but in both cases, the energy transfer rate was found to vary inversely with equilibrium fluctuations in the contact distance. Since that study, another computational study was carried out to examine this relation, this time for myoglobin at 300 K.[36] That work again found that, for nonbonded contacts interacting by short-range potentials, such as hydrogen bonded contacts, the energy transfer rate across the contact varies inversely with the variance in the contact length. For longer-range ionic contacts, the results were more ambiguous. A diffusion relation was found, whereby the energy transfer rate depends in a diffusive-like fashion on the distance between the ionic contacts. However, it was unlikely from the data that the rate of energy transfer across the contact varies inversely with the equilibrium fluctuations in the contact length, possibly due to several contacts interacting significantly with each other, rather than just a pair via, say, one hydrogen bond. The generality of the scaling between energy transfer rate and contact fluctuations at equilibrium is currently still under investigation.

Here we illustrate the scaling relation between rates of energy transfer across nonbonded contacts and equilibrium fluctuations of the contact for hydrogen bonded residues of the dimeric hemoglobin from *Scapharca inaequivalvis*, HbI, one of the proteins presented in Figure 1. The comparison of equilibrium fluctuations and energy transfer rates is made using the same trajectory from a molecular simulation. We have done this conveniently using the current calculation for proteins (CURP) computational approach developed by Yamato and co-workers.[55,150,151] The CURP calculation provides a local energy conductivity, G, between residue pairs, applying the Kubo relation between thermal conductivity and equilibrium energy fluctuations, and is analogous to the local energy diffusivity discussed above. Formally, they are related, as the local conductivity is given by the product of the local energy diffusivity and the heat capacity. The advantage of calculating the local energy conductivity using CURP to study relations between energy transfer across a nonbonded contact and fluctuations in the length of the contact is that both properties can be calculated using the same equilibrium MD trajectory. We note that energy conductivity, G, obtained from the time-correlation function of the inter-residue energy current, as described elsewhere,[15,55,150] is multiplied by RT; values of G are given in $(\text{kcal mol}^{-1})^2\ \text{ps}^{-1}$.

In Figure 3, we plot G vs $\langle \delta r^2 \rangle^{-1}$ for polar contacts of HbI in the unliganded state. Polar contacts are defined as X–H···O, where X was taken to be either N or O and the H···Oseparation is no greater than 2.8 Å. Hydrogen bonds, a subclass of polar contacts, were selected for angles XHO $\geq 150°$. Polar contacts were considered for further analysis if the contact criteria were met for 99% of the trajectory. For all contacts existing over the entire trajectory, the average distance between the O and H involved in the polar contact, $\langle r \rangle$, and the variance in the distance, $\langle \delta r^2 \rangle = \langle (r - \langle r \rangle)^2 \rangle$, were calculated and subsequently paired with the respective energy conductivity, G, computed for this trajectory. We note that, to eliminate trajectories with small G and reduce the noise at small $\langle \delta r^2 \rangle^{-1}$, we only plot data with G exceeding a threshold of 50 $(\text{kcal mol}^{-1})^2\ \text{ps}^{-1}$.

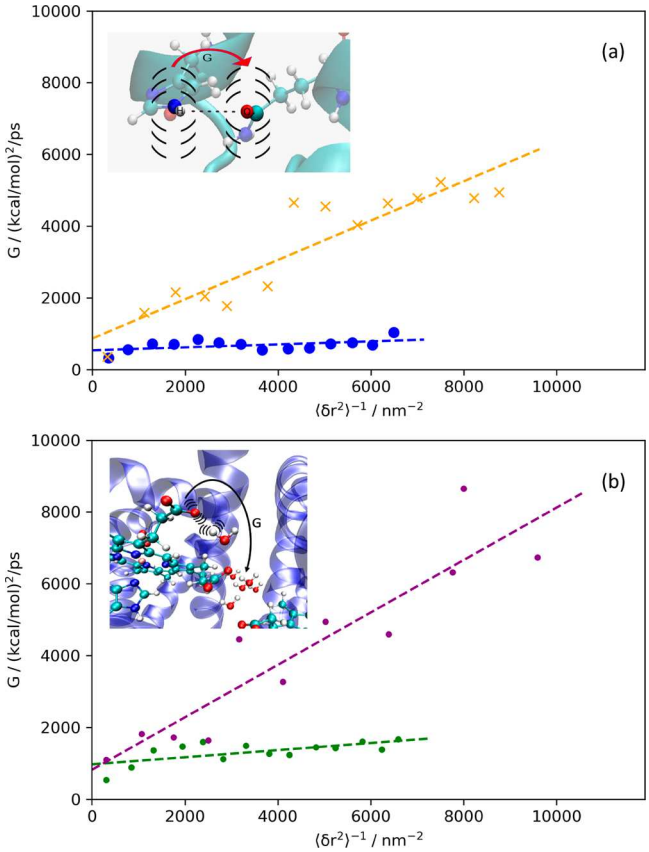

Figure 3. (a) Energy conductivity, G, across polar contacts of deoxy-HbI as a function of the inverse of the variance, $\langle \delta r^2 \rangle^{-1}$, in the length of that contact. The data appear to fall on two lines for different sets of polar contacts. (b) Energy conductivity, G, between the cluster of water molecules at the interface of deoxy-HbI and either the heme or residues at the interface as a function of the inverse of the variance, $\langle \delta r^2 \rangle^{-1}$, in the length of that contact. The data plotted in purple, which fall near the line with greater slope, correspond to hydrogen bonding between the heme and water molecules at the interface. The data plotted in green correspond to hydrogen bonding between interface water molecules and either lysine or arginine. The insets to parts a and b are schematic illustrations of the relation between fluctuations in the distance of a hydrogen bond and the rate of energy transfer between hydrogen bonded residues, as quantified by the energy conductivity, G.

In Figure 3a, we plot the results for polar contacts within each globule of deoxy-HbI, which are nearly all hydrogen bonds, while, in Figure 3b, we plot the results for contacts between the interface water cluster and either the heme (purple) or residues at the interface (green) that strongly couple to the water, specifically side chains of lysine and arginine. The polar contacts plotted in Figure 3a do not include hydrogen bonds along α-helices, as energy transport along α-helices follows the rule for energy transport along the main chain mentioned above.[35] In Figure 3a, we observe that the computational data for G across hydrogen bonds in each globule fall along two different lines, a result we found earlier for polar contacts in myoglobin.[36] The data labeled in orange and those in blue correspond to the contacts plotted with these respective colors for myoglobin, listed in ref 36. The data for contacts with water exhibit an energy conductivity that is comparable to that found for energy transfer between residue pairs, even larger for the case of heme–water. Overall, since G is proportional to the energy transfer rate, w, the data plotted in Figure 3 support the scaling of energy

DOI: 10.1021/acs.jpcb.9b07086
J. Phys. Chem. B 2019, 123, 9507–9524

transfer rates with fluctuations around the average distance between the polar contact, i.e., $w \propto \langle \delta r^2 \rangle^{-1}$.

As noted, we do not yet know how general the scaling of the energy transfer rate with equilibrium contact fluctuations is, only that we have found it to hold for short-range interactions we have studied thus far. For longer-range ionic contacts, results we obtained for myoglobin were less clear.[36] We found in that case that the rate of energy transfer is consistent with a diffusion equation, which in turn depends on the number of contacts that simultaneously interact with one another. Work on energy transfer across nonbonded contacts is ongoing.

It is interesting to consider further the relation between equilibrium dynamics and energy transfer when the relation $w \propto \langle \delta r^2 \rangle^{-1}$ holds. A change in functional state, or a mutation, could lead to a change in dynamics of a contact. We assume for now that the contact is maintained for a given functional state, at least for a very high percent of the time. The change in dynamics with change in functional state (or mutation), in turn, corresponds to a change in the rate of energy transfer across the contact. The energy transfer rate across a contact can be measured by time-resolved vibrational spectroscopy, which could thereby provide information about the change in dynamics with change in functional state or mutation. The same measurement can provide information about a change in entropy associated with the change in local dynamics. At fixed temperature, the change in entropy, ΔS, associated with the change in dynamics of the nonbonded contact going from state 1 to 2, with change in force constant from f_1 to f_2, is $\Delta S = \frac{k_B}{2} \ln\left(\frac{f_1}{f_2}\right) = k_B \ln\left(\frac{\omega_1}{\omega_2}\right)$ in the harmonic approximation. Since in that approximation the energy transfer rate is proportional to the force constant, we have $\Delta S = \frac{k_B}{2} \ln\left(\frac{w_1}{w_2}\right)$.

If the vibrational energy transfer rate across the contact can be measured prior to, w_1, and following, w_2, a change in functional state, we can learn about changes in the entropy associated with the dynamics of that contact caused by that state change.[36] Of course, there may be many other changes in dynamics that would contribute to differences in entropy between the two states. Such a measurement only provides information associated with the dynamics of one contact, and while that appears more restrictive than NMR measurements that yield information about changes in methyl rotor dynamics and their associated entropy change with change in functional state,[152−157] it can also pinpoint a contribution from a change in one region.

As an example, time-resolved Raman experiments carried out by Mizutani and co-workers indicate that energy transfer from the heme to Trp68, which are tightly packed together, is not influenced by cleavage of the heme from the proximal histidine, His93, a H93G mutant.[69] MD simulations reveal that the packing and dynamics between the heme and Trp68 do not change noticeably in going from myoglobin to the H93G mutant.[69] Mizutani and co-workers find that the energy transfer kinetics from the heme into the protein via Trp68 is not influenced by the changes around other parts of the heme that leave intact the contact between the heme and Trp68. This observation is consistent with the close connection between energy transfer rate across a nonbonded contact interacting by a short-range potential, in this case a van der Waals interaction, and the dynamics of the contact. The energy transfer rate is seen to be unchanged as long as the contact structure and dynamics do not change with the mutation, highlighting the importance of nonbonded contacts in energy redistribution and protein stability.

4. THERMAL CONDUCTANCE OF THE PROTEIN−WATER INTERFACE

We discuss here energy transport between protein and solvent from a more coarse-grained perspective than in the previous sections. To assess the role of solvent in energy transfer between a protein and its environment, it is useful to consider the case of the two systems at different temperature and examine thermal transport across the protein−water interface. Thermal boundary conductance between protein and solvent has been calculated by molecular simulations and theoretical modeling.[57,79−81,158] In earlier work, thermal boundary conductance was estimated using plausible values to explain time-resolved spectroscopic experiments of energy transfer in heme proteins,[159] where in this and other studies it was apparent that the boundary resistance between protein and water is rather small.[7,8] We discuss the relative thermal resistance within a protein to the resistance at the protein−water interface here. Overall, thermal diffusion through a protein into water is not impeded by the boundary between them. However, a protein may be insulated from thermal stress in its environment by the presence of other molecules at the interface, such as trehalose and other saccharides.[160,161] We have thus considered thermal conductance of a protein−saccharide−water interface, which we compare with thermal transport at the interface between protein and water.

Consider first the coefficient of thermal conductivity of a protein itself. Thermal transport coefficients for several proteins have been computed in linear response approximation, yielding values around 0.2 W m^{-1} K^{-1}.[81,126] The thermal conductivity of myoglobin has been measured by femtosecond time-resolved thermoreflectance techniques, revealing quantitative agreement with theoretical predictions over a wide range of temperature.[128] Moreover, the temperature dependence of the thermal conductivity is consistent with the enhancement of thermal transport by anharmonic interactions, which had been predicted in earlier theoretical and computational work.[72] As a reference, the thermal conductivity of proteins is about twice that of many organic materials but smaller than the thermal conductivity of water, about 0.6 W m^{-1} K^{-1}. We consider now thermal conductance of the protein−water interface.

We have calculated the thermal boundary conductance, h_{Bd}, for cytochrome *c* and water, myoglobin and water, and GFP and water[57,79,80] and plot the results in Figure 4. Values of the former two are within about 1% of each other, while values for GFP−water are about 10% larger. For the cytochrome *c*−water and myoglobin−water interfaces, we find a modest increase in boundary conductance over the plotted range of temperature, from about 240 MW K^{-1} m^{-2} at 200 K to about 315 MW K^{-1} m^{-2} at 340 K. This compares with about 265 MW K^{-1} m^{-2} at 200 K to about 340 MW K^{-1} m^{-2} at 340 K for the GFP−water interface. The values that we compute at 300 K are reasonably consistent with those computed for four different proteins (including GFP and myoglobin) by molecular simulations at 300 K, reported in ref 81. The calculations that yield the results plotted in Figure 4 are not all that sensitive to the force field models used for either protein or water, as long as each provides reasonable descriptions of the vibrational density of states in thermally accessible regions and the speed of sound. Those calculations adopted CHARMM potentials for the proteins and the TIP3P water model. The speed of sound in both protein[72]

DOI: 10.1021/acs.jpcb.9b07086
J. Phys. Chem. B 2019, 123, 9507−9524

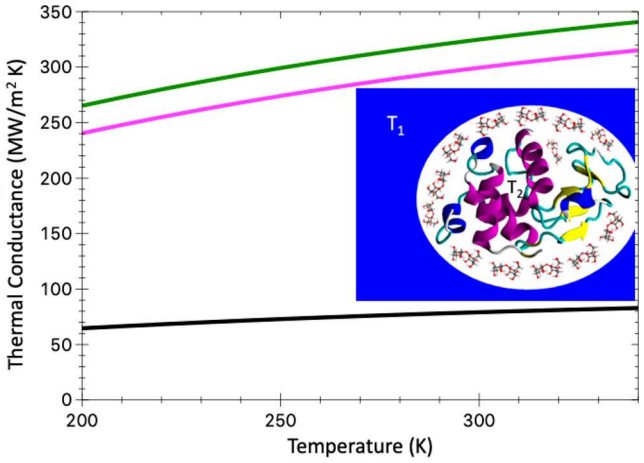

Figure 4. Thermal boundary conductance calculated for myoglobin and water and cytochrome *c* and water (magenta; the results for both are the same to within 1%) and GFP and water (green). Values above 100 MW/m^2 K are often larger than the thermal boundary conductance between many solid-state materials and correspond to little thermal resistance between a protein and its solvent environment, as discussed in the text. Introducing a saccharide layer, illustrated in the inset, between a protein and water substantially reduces thermal conductance (black).

and water[162] and their densities of states are modeled sufficiently well to provide good estimates to the boundary conductance in the plotted temperature range.

Vibrational energy transport across the protein−water interface is relatively efficient compared with interfaces involving other organic molecules that hydrogen bond to water. For example, the thermal boundary conductance between myoglobin, cytochrome *c*, and GFP and water is roughly 2−3 times as large as the thermal boundary conductance computed for the interface between water and a monolayer of hydrocarbon chains with −OH head groups.[163]

As noted, saccharides protect a protein from sudden change in ambient temperature. There has been much interest in dynamic and spectroscopic properties of saccharide−solvent interfaces,[164,165] and recently, we have calculated thermal transport properties of a number of saccharides and thermal conductance of the protein−trehalose−water interface, which we plot in Figure 4. As seen in the figure, near 300 K, the thermal boundary conductance for the protein−water interface is about 300 MW m^{-2} K^{-1}.[57,81] With a layer of trehalose, the thermal boundary conductance drops to about 80 MW m^{-2} K^{-1}. Compared to other organic molecules of similar size, some of which are presented in the following section, trehalose acts as a very effective organic insulator. It is also interesting to compare the contribution of a layer of saccharides to thermal transport between protein and water with the contribution of a cluster of water molecules between the two globules of the dimeric hemoglobin discussed in the previous section. We have found that for disaccharides the energy diffusion coefficient is smaller than that for water clusters and bulk water,[82] due to a smaller mean free path for vibrational energy diffusion at comparable frequency. There is thus greater resistance to thermal transport through a layer of disaccharides such as trehalose than there is through a cluster of water molecules.

The ratio of thermal resistance within a protein molecule to thermal resistance at the protein−water interface is given by the dimensionless Biot number, Bi, defined as Bi = $h_{Bd}L/\kappa$, where L is a length scale, often taken as the volume to surface area, κ is the coefficient of thermal conductivity, and h_{Bd} is the thermal boundary conductance. A Biot number roughly 0.1 or smaller indicates that thermal resistance at the interface is significantly larger than that within the protein, and roughly 1 or greater indicates relatively large interface conductance. At 300 K, we find $h_{Bd} \approx 300$ MW K^{-1} m^{-2} for the three proteins in Figure 4. For the thermal conductivity of a protein, we use as a representative value κ = 0.2 W K^{-1} m^{-1}, calculated[126] and measured[128] for myoglobin. We approximate the length, L, as the volume to surface area, $R/3$, which, using a 16 Å radius of gyration, roughly that of myoglobin, is about 0.5 nm. These estimates yield a value for the Biot number of Bi ≈ 0.75, so that thermal resistance at the protein−water interface is comparable to thermal resistance in the protein. With a layer of trehalose at the interface, the boundary conductance drops to 80 MW m^{-2} K^{-1} and the Biot number to 0.2, consistent with an interface that exhibits greater thermal resistance than the thermal resistance within the protein itself. From this discussion comparing two interfaces out of the diversity of interfaces that can exist at one time on the surface of the protein in a native environment, we see the implications of sugars providing a barrier to heat shock *in vivo*.

5. THERMAL CONDUCTANCE OF MOLECULAR INTERFACES

Insertion of a layer of small molecules between two large objects that act as thermal baths may impede or sometimes facilitate thermal conductance across the interface. For the protein−water interface, we find that a layer of saccharides introduces significant thermal boundary resistance. However, it is also possible to enhance thermal conductance between two thermal reservoirs by introduction of a molecular layer, as we shall see here. In this section, we focus less on biomolecules and more on properties of molecular interfaces or molecular junctions that mediate thermal boundary conductance. Thermal transport at molecular interfaces is currently studied for a wide range of systems.[166−182] Those that we address here, while not exclusively biomolecules, can be applied to biological systems, including gold nanoparticles (GNPs), which may be functionalized for photothermal applications in the cell.[74,102,104,183,184]

A variety of properties control the thermal conductance of interfaces, such as an interface of small molecules separating two relatively large objects held at reasonably well-defined temperature, which act as thermal baths. The protein−saccharide−water system discussed above serves as an example. Contacts and interactions between the molecular layer and substrates contribute to thermal conductance of the interface, as seen in experimental and computational work probing this effect.[163,185] In addition to the contacts, the composition, size, structure, and dynamics of the molecules at the interface also dictate thermal flow. Whether or not energy relaxes in a molecule at the interface between two thermal baths has a large impact on thermal boundary conductance.

The insets in Figure 5 illustrate the kinds of systems we consider. One consists of a monolayer of PEG oligomers capping a gold nanoparticle (GNP) in an aqueous environment. GNPs may be applied in a number of photothermal therapies, such as drug delivery and control of protein structure and aggregation.[74,102,104,183,184] To further examine effects of PEG oligomers at interfaces, we also consider a layer of PEG oligomers between two solid-state objects, one at temperature T_1 and the other at T_2. Thermal transport of molecular

DOI: 10.1021/acs.jpcb.9b07086
J. Phys. Chem. B 2019, 123, 9507−9524

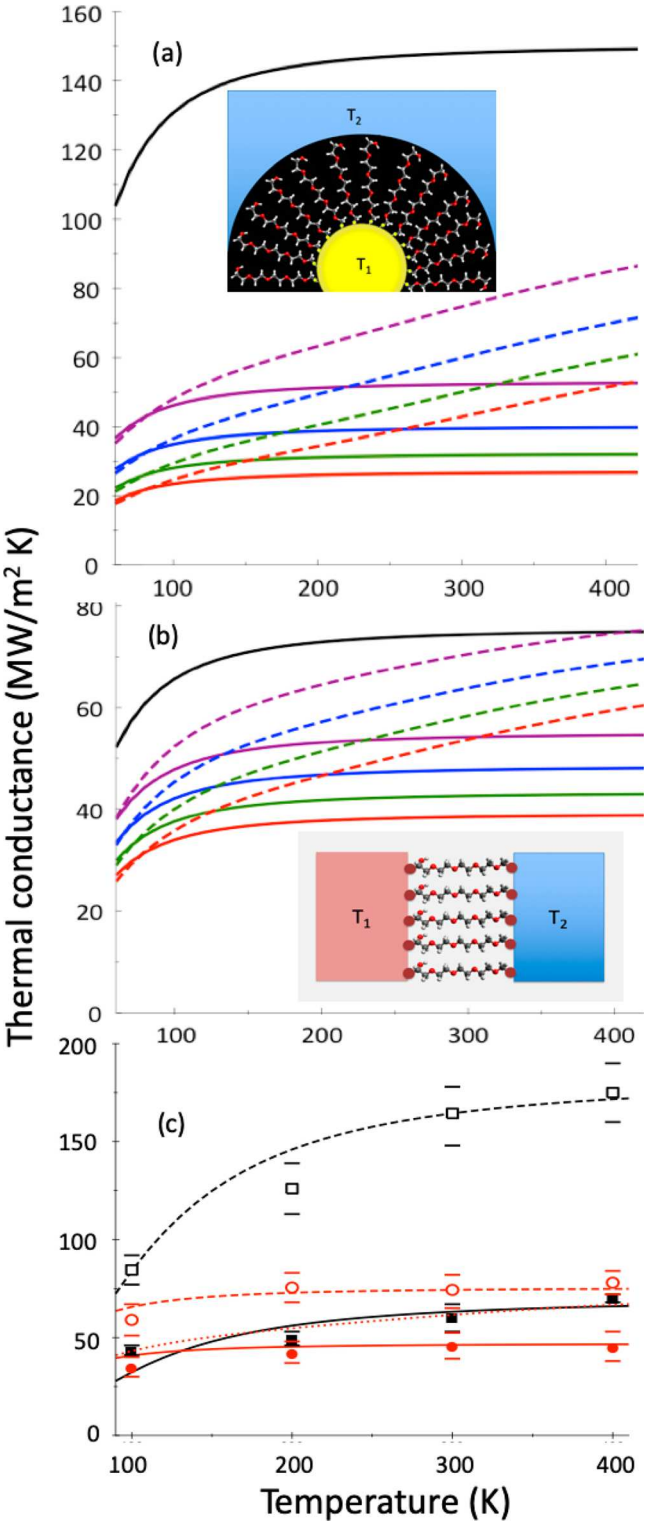

Figure 5. (a) Thermal boundary conductance between Au and water (black) and the thermal boundary conductance with a layer of PEG_4 (violet), PEG_6 (blue), PEG_8 (green), and PEG_{10} (red) between Au and water, where calculations were carried out with anharmonic interactions neglected (solid curves) and assumed to be large (dashed curves), representing no and rapid energy redistribution, respectively. Inset: Illustration of a gold nanoparticle (GNP), separated from the surrounding medium, which could be water, by a capping layer of PEG_n, $n = 4$, where each PEG oligomer is attached to a gold nanoparticle via a thiol–gold bond. The temperature of the GNP is T_1 and the surrounding medium T_2. (b) Thermal boundary conductance between Au and sapphire (black) and the thermal boundary conductance with a layer of PEG_4 (violet), PEG_6 (blue), PEG_8 (green), and PEG_{10} (red) between Au and sapphire, where calculations were carried out with anharmonic interactions neglected (solid curves) and assumed to be large (dashed curves). Inset: Two objects at different temperature, T_1 and T_2, with the molecular interface made up of PEG_n, $n = 4$. Red circles indicate bonding between the PEG oligomers and the substrates. (c) Calculations of thermal conductance between Au and sapphire (red) and between Al and sapphire (black) with an alkane chain (dashed) or fluorinated alkane (solid) interface for temperatures from 100 to 400 K. Experimental results from ref 173 are plotted (Au-sapphire red circles, Al-sapphire black squares, closed and open, respectively, for carbon-chain molecular interfaces that are fluorinated and not fluorinated) with reported error bars. Only elastic scattering is accounted for in the calculated results, apart from the dotted red curve, for which strong inelastic scattering leading to thermalization in the molecular interface is assumed, a result that clearly does not match the temperature-dependent experimental data. The experimental results are consistent with incomplete thermalization in these molecules to at least 2 nm. Parts a and b were reprinted with permission from ref 87. Copyright 2017 American Institute of Physics. Part c was reprinted with permission from ref 88. Copyright 2016 American Chemical Society.

monolayers between solid objects has been the subject of numerous experimental studies, many including alkanes and derivatives, providing data against which computational results can be compared.[172−174,185−187] The theoretical and computational studies in turn provide insights into the underlying mechanisms that control thermal conductance of a molecular interface.

Thermal conductance of the interface is influenced by contributions of elastic and inelastic scattering within the molecular layer. Elastic scattering is dictated by molecular structure and composition, and inelastic scattering, by anharmonic interactions and contact with the substrates. Both contribute to thermal transport dynamics, which may be at one extreme ballistic, when scattering is very weak, or otherwise diffusive. Thermalization in the molecules, which when sufficiently rapid yields a well-defined local temperature, is controlled by inelastic scattering. The nanometer length scale of a molecular interface can accommodate ballistic transport,[188−191] and even if transport is diffusive, anharmonic interactions may not yield sufficiently rapid energy relaxation for local temperature to be well-defined within the molecules at the interface or in a molecular junction. Either way, thermal transport may not adhere to Fourier's heat law on the molecular scale.

Consider first gold–PEG_n–water, n = 4, 6, 8, 10, plotted in Figure 5a, where we also plot the thermal boundary conductance calculated for a gold–water interface for comparison. The thermal boundary conductance has been calculated in two limits, one where inelastic scattering via anharmonic interactions is neglected (solid curves) and the other limit of rapid thermalization so that local temperature throughout the molecule is well-defined. While neither limit strictly holds, calculated rates of anharmonic decay of vibrational states in PEG oligomers the size of those plotted in Figure 5 are consistent with rapid anharmonic decay and thermalization on short (atomic) length scales.[87] We thus expect that thermal boundary conductance of the gold–PEG_n–water interface is described by the calculations that account for rapid energy redistribution in the PEG oligomers. We observe that thermalization enhances

DOI: 10.1021/acs.jpcb.9b07086
J. Phys. Chem. B 2019, 123, 9507−9524

thermal conductance of the boundary compared to systems of molecules in which it is very slow.

Thermal conductance of the gold−PEG_n−sapphire system, n = 4−10, is plotted in Figure 5b. The results are qualitatively similar to those for gold−PEG_n−water. However, in this case, we find that, when energy redistribution in the PEG oligomers is rapid, thermal conductance of the interface can exceed that of the thermal boundary conductance of gold−sapphire at higher temperatures.

Energy redistribution enhances thermal conduction because additional transport channels become available within the molecules at the interface, particularly at higher temperature. Phonons from gold that enter the molecule can upconvert to higher-frequency vibrations of the PEG oligomers, resulting in additional energy transfer to sapphire. Those channels are unavailable in the absence of thermalization. They are also unavailable in the absence of the molecular interface, which, when energy rearrangement occurs, can enhance thermal boundary conductance beyond that of the substrate−substrate interface. This is seen for gold−sapphire at temperatures of 400 K and beyond. A layer of PEG oligomers, in which energy redistribution is quite rapid, yields a thermal boundary conductance at the gold−PEG_n−sapphire interface that is greater than that for gold−sapphire when n is not very large at 400 K and higher and at higher temperatures when n is larger. Higher temperature enhances the rate of energy redistribution and amplifies the enhancement of thermal conductance by the molecular layer. For larger n, the overall resistance of the layer due to structural effects and elastic scattering is greater, so that higher temperature is needed to obtain the enhancement. We note that extremely rapid energy redistribution may yield a turnover effect, in which the mean free path becomes shorter as temperature increases, giving rise to a lower conductance.[180] That effect lies outside the temperature range for the systems plotted in Figure 5.

In contrast to PEG oligomers, computational studies of alkane chains have found them to exhibit relatively slow energy redistribution by anharmonic interactions, so that the length over which inelastic scattering occurs reaches tens of nm.[88,192] Indeed, recent measurements of thermal conductance of alkane chain junctions indicate that the conductance is independent of chain length,[193] consistent with ballistic transport and minimal effects of scattering seen in the calculations and other experiments.[88,174,192]

Thermal transport efficiency can be altered by alkane derivatives. Experiments measuring the thermal boundary conductance of a gold−sapphire interface have also been carried out with introduction of alkane and ∼2 nm fluorinated alkane monolayers.[173] Measurements on the fluorinated carbon monolayer system revealed smaller values of the thermal boundary conductance between gold and sapphire than for the interface without the molecular monolayer, in contrast to alkane chain monolayers, which apparently has no significant effect on thermal boundary conductance. The mechanism for thermal resistance was conjectured on the basis of that study to arise from anharmonic interactions in the molecules[173] but in fact could also be due to elastic scattering or both.

We subsequently carried out computational work to assess the relative importance of anharmonic interactions, which give rise to inelastic scattering, and structural effects of the molecular monolayer, which give rise to elastic scattering.[87,88] The calculations revealed that, while inelastic scattering in fluorinated alkanes is far more prevalent than in alkane chains, it is not sufficiently rapid to explain the temperature dependence of the experimentally measured thermal conductance from 100 to 400 K. The results of the computational study, along with the experimental measurements, are plotted in Figure 5c. The black and red dashed curves represent the computed thermal boundary conductance between aluminum and sapphire and gold and sapphire, respectively, with an alkane chain monolayer in between. The calculations provide a good match to the experimental results.[173] Those results are about the same whether or not the molecular monolayer is present between the metal and sapphire, indicating little thermal resistance of the alkane chain on the nanometer length scale from 100 to 400 K, consistent with the calculations as well as previous experimental measurements.[174,194]

Thermal boundary conductance computed for a 2 nm monolayer of fluorinated alkanes between aluminum and sapphire and gold and sapphire is also plotted in Figure 5c as solid black and red curves, respectively. For the calculations of thermal transport in these systems, we accounted for elastic scattering but neglected inelastic scattering due to anharmonic interactions, which, as already noted, was found in separate calculations to be insufficiently rapid to significantly influence thermal transport over a length of about 2 nm. The calculations of thermal conductance are seen to match the measured values quite well from 100 to 400 K, indicating that the thermal resistance in the fluorinated alkanes that is observed in the experiments indeed arises from elastic scattering in the molecules. In fact, if we carry out the calculation of thermal boundary conductance between gold and sapphire through a fluorinated alkane monolayer by introducing artificially large inelastic scattering rates, we find a more rapid rise in thermal conductance with increasing temperature, indicated in Figure 5c as the dotted red curve, than seen in the experimental measurements.

6. SUMMARY AND FUTURE DIRECTIONS

Contributions of structure and equilibrium dynamics to energy transport through biomolecules and across interfaces with their surroundings are becoming clearer through a combination of theory, computational studies, and experiment. In this Feature Article, we have discussed networks of energy transport in systems of biological molecules, where we have focused on proteins, saccharides, and surrounding and embedded water, in particular the role of interfaces between different chemical groups, molecules, and materials. While these systems explore a range of structures during function, the sub-nanosecond, vibrational time scales we consider restrict the networks over which energy transport occurs. Energy transport along the network depends on a number of properties, including molecular structure, equilibrium fluctuations of nonbonded contacts, and energy relaxation and thermalization within the network. We have discussed recent work exploring the use of master equation simulations to model energy transport in systems of biological molecules, connections between energy transfer across molecular interfaces and equilibrium fluctuations of the interface, and thermal transport through molecular interfaces in biological systems.

Although energy is transported by modes that span a range of length scales,[72,73] we have nevertheless found that a Markov approximation on the scale of residues and a master equation predict energy transport quite well when compared with results of all-atom simulations.[35,37] Recent work has examined connections between equilibrium structural fluctuations and

DOI: 10.1021/acs.jpcb.9b07086
J. Phys. Chem. B 2019, 123, 9507−9524

rates of energy transfer across nonbonded contacts, which help identify values of rate constants in a master equation. For short-range contacts, such as hydrogen bonds, we have thus far found the scaling between energy transfer rate and inverse in the variance of contact length to hold up well. For long-range ionic contacts, a diffusion picture is supported by computational results, but simultaneous interactions appear to complicate the short-range relation between energy transfer rate and equilibrium structural fluctuations, which is not as simple as the case of hydrogen bonds studied to date.[36] Those, too, may reveal more complicated trends if the residues that are in contact are involved in several hydrogen bonded interactions. Overall, the scope of applicability of the relations between equilibrium structural fluctuations and energy transfer along the network, identified for hydrogen bonds in myoglobin and HP36 and van der Waals contacts in HP36,[35,36] remains to be more firmly established for proteins, proteins and water, and at other interfaces. To the extent that rates of energy transfer across an interface are related to equilibrium fluctuations of the contact, measurements of energy transfer rates by time-resolved vibrational spectroscopy provide insight into the dynamics and associated entropy of the contact, in particular changes associated with change in functional state or mutation. We have discussed above some recent experiments that appear to be consistent with this picture, but further studies are needed.

We have also discussed the related topic of thermal conductance of a variety of molecular interfaces relevant to biological systems. Energy and thermal transport between proteins and water, while facile at the protein−water interface, can be modified with a layer of small molecules at the interface between them. Saccharides, in particular trehalose, provide an insulating layer that is consistent with their ability, and those of larger saccharides, to protect proteins and preserve function when proteins are exposed to a number of stresses including thermal effects.

Small molecules at the interface between two materials, each at fixed temperature, mediate thermal conductance of the interface due to a number of properties, including their structure, composition, and dynamics, as well as interactions between the molecules and substrates. The rate of energy relaxation within the molecules at the interface plays a critical role in thermal boundary conductance.[89] Relaxation may enhance thermal conductance, as it allows energy rearrangement within the molecules, which can bridge a mismatch in the vibrational density of states of the two heat baths. We have seen a substantial enhancement, particularly at higher temperature, of the thermal boundary conductance between gold and other materials with a higher Debye temperature when energy relaxation within the molecules that bridge them is rapid. Conversely, if energy relaxation is limited and slow, the temperature dependence of the conductance is more muted and the density of states mismatch of the two leads cannot be partially offset by the molecular interface. While not found for the systems discussed here, it is also possible that energy redistribution due to anharmonic interactions can be so rapid that it introduces resistance to thermal transport at the interface.[180]

The role of energy relaxation and thermalization in molecules at interfaces on thermal conductance of molecular junctions and interfaces, as well as effects of structure and composition, still need further study for a more quantitative description and control of thermal properties, essential to applications such as thermally controlled charge transfer,[195−197] photothermal activation of drug delivery and structural changes of proteins and nucleic acids in cells,[102] and energy and thermal rectification through molecules.[80,86,179,198−206] Biologically inspired materials may also exhibit interesting and useful thermal properties. Recent measurements of a protein-like oligomeric system found the thermal conductivity of the material could be tuned by a remarkable factor of about 2.5 by rapid and reversible hydration and dehydration.[187] Further study and understanding of properties that control thermal transport in this and other biologically inspired systems may lead to new materials with adjustable thermal properties.

We have seen that structure and equilibrium dynamics can serve as predictors for the anisotropic response of impulsive excitation in a system of biological molecules. Detailed pictures of how vibrational and vibronic relaxation through a protein and its surroundings influence the dynamics and kinetics of chemical reactions occurring on the 1 or 10 ps time scale, including photochemical isomerization and charge transfer reactions in protein photosensors, have emerged for some time.[4,5,207−210] To what extent the response on vibrational time scales is an indicator of structural changes that may occur over longer times during allosteric transitions or in molecular motors,[211−213] among others, still needs to be explored. The rapid, vibrational response in a system of protein and water has been found in some nonequilibrium molecular simulations to serve as a useful predictor;[18,22] in other cases, it is less clear,[21,214] and the extent and limitations of such connections require further study.

AUTHOR INFORMATION

Corresponding Author

*E-mail: dml@unr.edu.

ORCID

David M. Leitner: 0000-0002-3105-818X

Present Address

†H.D.P.: Department of Chemistry, University of California Riverside, Riverside, CA 92521.

Notes

The authors declare no competing financial interest.

Biographies

David M. Leitner is Reynold C. Fuson Professor of Chemistry at the University of Nevada, Reno. His current research interests include theoretical and computational studies of energy flow in molecules, particularly in biological systems, and its influence on chemical reaction kinetics. Other areas include theoretical approaches to address thermal transport in nanoscale systems and computational studies of terahertz spectroscopy and dynamics of solvated biomolecules. He carried out his undergraduate studies in Chemical Engineering and Chemistry at Cornell University and received his Ph.D. in Chemical Physics at the University of Chicago working with R. S. Berry. He was an NSF Postdoctoral Fellow and Alexander von Humboldt Fellow at the University of Heidelberg, where he worked with Lorenz Cederbaum, a research associate at the University of Illinois at Urbana−Champaign, where he worked with Peter Wolynes, and assistant project scientist at UCSD prior to joining the Chemistry Department at UNR in 2000. He is a Fellow of the American Physical Society and Fellow of the American Association for the Advancement of Science.

Hari Datt Pandey received his B.Sc. in Physics, Chemistry, and Mathematics and M.Sc. in Mathematics from Tribhuvan University in Nepal. He then moved to the University of Nevada, Reno, where he first pursued his M.S. in Mathematics and then entered the Chemical Physics Ph.D. program working in the research group of Prof. David M.

DOI: 10.1021/acs.jpcb.9b07086
J. Phys. Chem. B 2019, 123, 9507−9524

Leitner. Hari performed theoretical and computational studies of nanoscale heat and energy transport, vibrational relaxation in molecules, and studies of thermodynamics of large molecular systems in his graduate research. Since August 2018, he has been working as a postdoctoral researcher at the University of California, Riverside, in the group of Prof. Chia-en Chang, where he is studying the thermodynamics of proteins, binding kinetics, molecular recognition, and drug discovery.

Korey M. Reid received his B.S. in Chemistry from the University of California, Davis, in 2010. Following a stint in biomedical engineering where he researched eye pathology, he completed a M.S. in Chemistry under Prof. V. V. Krishnan at Fresno State in 2014 utilizing NMR and molecular dynamics to investigate intrinsically disordered peptides in a non-native solvent. Subsequently, he started his Ph.D. under Prof. David M. Leitner where his focus has been modeling protein dynamics and energy transport in biomolecular systems, with focus on the role of interfaces between biomolecules and water.

■ ACKNOWLEDGMENTS

We have enjoyed discussions and collaboration with Gerhard Stock and Takahisa Yamato on many aspects of this work. Some of it was carried out while D.M.L. was a Senior Fellow at the Freiburg Institute for Advanced Studies (FRIAS) and continues while D.M.L. is a JSPS Invitational Fellow at Nagoya University. Support from NSF grants CHE-1361776 and CHE-1854271 is gratefully acknowledged.

■ REFERENCES

(1) Leitner, D. M. Energy Flow in Proteins. *Annu. Rev. Phys. Chem.* **2008**, *59*, 233−259.
(2) Leitner, D. M.; Straub, J. E. *Proteins: Energy, Heat and Signal Flow*; CRC Press, Taylor & Francis Group: Boca Raton, FL, 2010.
(3) Nagy, A. M.; Raicu, V.; Miller, R. J. D. Nonlinear Optical Studies of Heme Protein Dynamics: Implications for Proteins as Hybrid States of Matter. *Biochim. Biophys. Acta, Proteins Proteomics* **2005**, *1749*, 148−172.
(4) Schoenlein, R. W.; Peteanu, L. A.; Mathies, R. A.; Shank, C. V. The First Step in Vision: Femtosecond Isomerization of Rhodopsin. *Science* **1991**, *254*, 412−415.
(5) Fang, C.; Frontiera, R. R.; Tran, R.; Mathies, R. A. Mapping Gfp Structure Evolution During Proton Transfer with Femtosecond Raman Spectroscopy. *Nature* **2009**, *462*, 200−205.
(6) Botan, V.; Backus, E. H. G.; Pfister, R.; Moretto, A.; Crisma, M.; Toniolo, C.; Nguyen, P. H.; Stock, G.; Hamm, P. Energy Transport in Peptide Helices. *Proc. Natl. Acad. Sci. U. S. A.* **2007**, *104*, 12749−12754.
(7) Lian, T.; Locke, B.; Kholodenko, Y.; Hochstrasser, R. M. Energy Flow from Solute to Solvent Probed by Femtosecond Ir Spectroscopy: Malachite Green and Heme Protein Solutions. *J. Phys. Chem.* **1994**, *98*, 11648−11656.
(8) Kholodenko, Y.; Volk, M.; Gooding, E.; Hochstrasser, R. M. Energy Dissipation and Relaxation Processes in Deoxymyoglobin after Photoexcitation in the Soret Region. *Chem. Phys.* **2000**, *259*, 71−87.
(9) Fayer, M. D. Fast Protein Dynamics Probed with Infrared Vibrational Echo Experiments. *Annu. Rev. Phys. Chem.* **2001**, *52*, 315−356.
(10) Barends, T. R. M.; Foucar, L.; Ardevol, A.; Nass, K.; Aquila, A.; Botha, S.; Doak, R. B.; Falahati, K.; Hartmann, E.; Hilpert, M.; et al. Direct Observation of Ultrafast Collective Motions in Co Myoglobin Upon Ligand Dissociation. *Science* **2015**, *350*, 445−450.
(11) Levantino, M.; Schiro, G.; Lemke, H. T.; Cottone, G.; Glownia, J. M.; Zhu, D.; Chollet, M.; Ihee, H.; Cupane, A.; Cammarata, M. Ultrafast Myoglobin Structural Dynamics Observed with an X-Ray Free-Electron Laser. *Nat. Commun.* **2015**, *6*, 6772.
(12) Liu, Y.; Guchhait, B.; Siebert, T.; Fingerhut, B. P.; Elsaesser, T. Molecular Couplings and Energy Exchange between DNA and Water Mapped by Femtosecond Infrared Spectroscopy of Backbone Vibrations. *Struct. Dyn.* **2017**, *4*, 044015.
(13) Balevicius, V.; Wei, T.; DiTommaso, D.; Abramavicius, D.; Hauer, J.; Polivka, T.; Duffy, C. D. P. The Full Dynamics of Energy Relaxation in Large Organic Molecules: From Photo-Excitation to Solvent Heating. *Chem. Sci.* **2019**, *10*, 4792−4804.
(14) Nguyen, P. H.; Hamm, P.; Stock, G. Nonequilibrium Molecular Dynamics Simulation of Photoinduced Energy Flow in Peptides: Theory Meets Experiment. In *Proteins: Energy, Heat and Signal Flow*; Leitner, D. M., Straub, J. E., Eds.; CRC Press, Taylor & Francis Group: Boca Raton, FL, 2010; pp 149−168.
(15) Leitner, D. M.; Yamato, T.; Parrill, A. L.; Lipkowitz, K. B. Mapping Energy Transport Networks in Proteins. *Rev. Comput. Chem.* **2018**, *31*, 63−114.
(16) Leitner, D. M.; Havenith, M.; Gruebele, M. Biomolecule Large Amplitude Motion and Solvation Dynamics: Modeling and Probes from Thz to X-Rays. *Int. Rev. Phys. Chem.* **2006**, *25*, 553−582.
(17) Leitner, D. M.; Gruebele, M.; Havenith, M. Solvation Dynamics of Biomolecules: Modeling and Terahertz Experiments. *HFSP J.* **2008**, *2*, 314−323.
(18) Ota, N.; Agard, D. A. Intramolecular Signaling Pathways Revealed by Modeling Anisotropic Thermal Diffusion. *J. Mol. Biol.* **2005**, *351*, 345−354.
(19) Kong, Y.; Karplus, M. Signaling Pathways of PDZ2 Domain: A Molecular Dynamics Interaction Correlation Analysis. *Proteins: Struct., Funct., Genet.* **2009**, *74*, 145−154.
(20) Laine, J. M.; Amat, M.; Morgan, B. R.; Royer, W. E.; Massi, F. Insight into the Allosteric Mechanism of Scapharca Dimeric Hemoglobin. *Biochemistry* **2014**, *53*, 7199−7210.
(21) Stock, G.; Hamm, P. A Nonequilibrium Approach to Allosteric Communication. *Philos. Trans. R. Soc., B* **2018**, *373*, 20170187.
(22) Smock, R. G.; Gierasch, L. M. Sending Signals Dynamically. *Science* **2009**, *324*, 198−203.
(23) Gulzar, A.; Valino-Borau, L.; Buchenberg, S.; Wolf, S.; Stock, G. Energy Transport Pathways in Proteins: A Nonequilibrium Molecular Dynamics Simulation Study. *J. Chem. Theory Comput.* **2019**, DOI: 10.1021/acs.jctc.9b00598.
(24) Sagnella, D. E.; Straub, J. E.; Thirumalai, D. Timescales and Pathways for Kinetic Energy Relaxation in Solvated Proteins: Application to Carbonmonoxy Myoglobin. *J. Chem. Phys.* **2000**, *113*, 7702−7711.
(25) Sagnella, D. E.; Straub, J. E. Directed Energy "Funneling" Mechanism for Heme Cooling Following Ligand Photolysis or Direct Excitation in Solvated Carbonmonoxy Myoglobin. *J. Phys. Chem. B* **2001**, *105*, 7057−7063.
(26) Bu, L.; Straub, J. E. Simulating Vibrational Energy Flow in Proteins: Relaxation Rate and Mechanism for Heme Cooling in Cytochrome C. *J. Phys. Chem. B* **2003**, *107*, 12339−12345.
(27) Takayanagi, M.; Okumura, H.; Nagaoka, M. Anisotropic Structural Relaxation and Its Correlation with the Excess Energy Diffusion in the Incipient Process of Photodissociated Mbco: High-Resolution Analysis Via Ensemble Perturbation Method. *J. Phys. Chem. B* **2007**, *111*, 864−869.
(28) Nagaoka, M.; Yu, I.; Takayanagi, M. Energy Flow Analysis in Proteins Via Ensemble Molecular Dynamics Simulations: Time-Resolved Vibrational Analysis and Surficial Kirkwood-Buff Theory. In *Proteins: Energy, Heat and Signal Flow*; Leitner, D. M., Straub, J. E., Eds.; Taylor & Francis Group, CRC Press: Boca Raton, FL, 2010; pp 169−196.
(29) Frauenfelder, H.; Sligar, S. G.; Wolynes, P. G. The Energy Landscapes and Motions of Proteins. *Science* **1991**, *254*, 1598−1603.
(30) Zhuravlev, P. I.; Papoian, G. A. Protein Functional Landscaoes, Dynamics, Allostery: A Tortuous Path Towards a Universal Theoretical Framework. *Q. Rev. Biophys.* **2010**, *43*, 295−332.
(31) Leitner, D. M. Vibrational Energy Transfer in Helices. *Phys. Rev. Lett.* **2001**, *87*, 188102.
(32) Leitner, D. M. Vibrational Energy Transfer and Heat Conduction in a One-Dimensional Glass. *Phys. Rev. B: Condens. Matter Mater. Phys.* **2001**, *64*, 094201.

DOI: 10.1021/acs.jpcb.9b07086
J. Phys. Chem. B 2019, 123, 9507−9524

(33) Leitner, D. M. Temperature Dependence of the Pure Vibrational Dephasing Rate in a Heteropolymer. *Chem. Phys. Lett.* **2002**, *359*, 434−439.
(34) Leitner, D. M. Anharmonic Decay of Vibrational States in Helical Peptides, Coils and One-Dimensional Glasses. *J. Phys. Chem. A* **2002**, *106*, 10870−10876.
(35) Buchenberg, S.; Leitner, D. M.; Stock, G. Scaling Rules for Vibrational Energy Transport in Proteins. *J. Phys. Chem. Lett.* **2016**, *7*, 25−30.
(36) Reid, K. M.; Yamato, T.; Leitner, D. M. Scaling of Rates of Vibrational Energy Transfer in Proteins with Equilibrium Dynamics and Entropy. *J. Phys. Chem. B* **2018**, *122*, 9331−9339.
(37) Leitner, D. M.; Buchenberg, S.; Brettel, P.; Stock, G. Vibrational Energy Flow in the Villin Headpiece Subdomain: Master Equation Simulations. *J. Chem. Phys.* **2015**, *142*, 075101.
(38) Yu, X.; Leitner, D. M. Anomalous Diffusion of Vibrational Energy in Proteins. *J. Chem. Phys.* **2003**, *119*, 12673−12679.
(39) Enright, M. B.; Yu, X.; Leitner, D. M. Hydration Dependence of the Mass Fractal Dimension and Anomalous Diffusion of Vibrational Energy in Proteins. *Phys. Rev. E* **2006**, *73*, 051905.
(40) Enright, M. B.; Leitner, D. M. Mass Fractal Dimension and the Compactness of Proteins. *Phys. Rev. E* **2005**, *71*, 011912.
(41) DiPaola, L.; Paci, P.; Santoni, D.; DeRuvo, M.; Giuliani, A. Proteins as Sponges: A Statistical Journey Along Protein Structure Organization Principles. *J. Chem. Inf. Model.* **2012**, *52*, 474−482.
(42) Banerji, A.; Ghosh, I. Fractal Symmetry of Protein Interior: What Have We Learned? *Cell. Mol. Life Sci.* **2011**, *68*, 2711−2737.
(43) DiPaola, L.; Giuliani, A. Protein Contact Network Topology: A Natural Language for Allostery. *Curr. Opin. Struct. Biol.* **2015**, *31*, 43−48.
(44) Banerji, A. *Fractal Symmetry of Protein Interior*; Springer: Basel, Switzerland, 2013.
(45) Banerji, A.; Ghosh, I. Revisiting the Myths of Protein Interior: Studying Proteins with Mass-Fractal Hydrophobicity Fractal and Polarizability-Fractal Dimensions. *PLoS One* **2009**, *4*, e7361.
(46) Chowdary, P.; Gruebele, M. Molecules: What Kind of Bag of Atoms? *J. Phys. Chem. A* **2009**, *113*, 13139−13143.
(47) Reuveni, S.; Klafter, J.; Granek, R. Dynamic Structure Factor of Vibrating Fractals. *Phys. Rev. Lett.* **2012**, *108*, 068101.
(48) Reuveni, S.; Granek, R.; Klafter, J. Anomalies in the Vibrational Dynamics of Proteins Are a Consequence of Fractal-Like Structure. *Proc. Natl. Acad. Sci. U. S. A.* **2010**, *107*, 13696−70.
(49) Granek, R.; Klafter, J. Fractons in Proteins: Can They Lead to Anomalously Decaying Time Autocorrelations? *Phys. Rev. Lett.* **2005**, *95*, 098106.
(50) Fujii, N.; Mizuno, M.; Ishikawa, H.; Mizutani, Y. Observing Vibrational Energy Flow in a Protein with the Spatial Resolution of a Single Amino Acid Residue. *J. Phys. Chem. Lett.* **2014**, *5*, 3269−3273.
(51) Baumann, T.; Hauf, M.; Schildhauer, F.; Eberl, K. B.; Durkin, P. M.; Deniz, E.; Loffler, J. G.; Acevedo-Rocha, C. G.; Jaric, J.; Martins, B. M.; et al. Observation of Site-Resolved Vibrational Energy Transfer Using a Genetically Encoded Ultrafast Heater. *Angew. Chem., Int. Ed.* **2019**, *58*, 2899−2903.
(52) Leitner, D. M. Water-Mediated Energy Dynamics in a Homodimeric Hemoglobin. *J. Phys. Chem. B* **2016**, *120*, 4019−4027.
(53) Gnanasekaran, R.; Agbo, J. K.; Leitner, D. M. Communication Maps Computed for Homodimeric Hemoglobin: Computational Study of Water-Mediated Energy Transport in Proteins. *J. Chem. Phys.* **2011**, *135*, No. 065103.
(54) Koike, K.; Kawaguchi, K.; Yamato, T. Stress Tensor Analysis of the Protein Quake of Photoactive Yellow Protein. *Phys. Chem. Chem. Phys.* **2008**, *10*, 1400−1405.
(55) Ishikura, T.; Yamato, T. Energy Transfer Pathways Relevant for Long-Range Intramolecular Signaling of Photosensory Protein Revealed by Microscopic Energy Conductivity Analysis. *Chem. Phys. Lett.* **2006**, *432*, 533−537.
(56) Agbo, J. K.; Gnanasekaran, R.; Leitner, D. M. Communication Maps: Exploring Energy Transport through Proteins and Water. *Isr. J. Chem.* **2014**, *54*, 1065−1073.
(57) Agbo, J. K.; Xu, Y.; Zhang, P.; Straub, J. E.; Leitner, D. M. Vibrational Energy Flow across Heme-Cytochrome c and Cytochrome c-Water Interfaces. *Theor. Chem. Acc.* **2014**, *133*, No. 1504.
(58) Leitner, D. M. Frequency Resolved Communication Maps for Proteins and Other Nanoscale Materials. *J. Chem. Phys.* **2009**, *130*, 195101.
(59) Gnanasekaran, R.; Xu, Y.; Leitner, D. M. Dynamics of Water Clusters Confined in Proteins: A Molecular Dynamics Simulation Study of Interfacial Waters in a Dimeric Hemoglobin. *J. Phys. Chem. B* **2010**, *114*, 16989−96.
(60) Wang, W. B.; Liang, Y.; Zhang, J.; Wu, Y. D.; Du, J. J.; Li, Q. M.; Zhu, J. Z.; Su, J. G. Energy Transport Pathway in Proteins: Insights from Non-Equilibrium Molecular Dynamics with Elastic Network Model. *Sci. Rep.* **2018**, *8*, 9487.
(61) Martínez, L.; Figueira, A. C. M.; Webb, P.; Polikarpov, I.; Skaf, M. S. Mapping the Intramolecular Vibrational Energy Flow in Proteins Reveals Functionally Important Residues. *J. Phys. Chem. Lett.* **2011**, *2*, 2073−2078.
(62) Maggi, L.; Carloni, P.; Rossetti, G. Vibrational Energy in Proteins Correlates with Tolopogy. *J. Phys. Chem. Lett.* **2018**, *9*, 6393−6398.
(63) Chennubhotla, C.; Bahar, I. Signal Propagation in Proteins and Relation to Equilibrium Fluctuations. *PLoS Comput. Biol.* **2007**, *3*, e172.
(64) Rajasekaran, N.; Sekhar, A.; Naganathan, A. N. A Universal Pattern in the Percolation and Dissipation of Protein Structural Perturbations. *J. Phys. Chem. Lett.* **2017**, *8*, 4779−4784.
(65) Naganathan, A. N. Modulation of Allosteric Coupling by Mutations: From Protein Dynamics and Packing to Altered Native Ensembles and Function. *Curr. Opin. Struct. Biol.* **2019**, *54*, 1−9.
(66) Brinkmann, L. U. L.; Hub, J. S. Ultrafast Anisotropic Protein Quake Propagation after Co Photodissociation in Myoglobin. *Proc. Natl. Acad. Sci. U. S. A.* **2016**, *113*, 10565−10570.
(67) Ota, K.; Yamato, T. Energy Exchange Network Model Demonstrates Protein Allosteric Transition: An Application to an Oxygen Sensor Protein. *J. Phys. Chem. B* **2019**, *123*, 768−775.
(68) Müller-Werkmeister, H. M.; Bredenbeck, J. A Donor-Acceptor Pair for the Real Time Study of Vibrational Energy Transfer in Proteins. *Phys. Chem. Chem. Phys.* **2014**, *16*, 3261−3266.
(69) Yamashita, S.; Mizuno, M.; Tran, D. P.; Dokainish, H.; Kitao, A.; Mizutani, Y. Vibrational Energy Transfer from Heme through Atomic Contacts in Proteins. *J. Phys. Chem. B* **2018**, *122*, 5877−5884.
(70) Mizutani, Y. Time-Resolved Resonance Raman Spectroscopy and Application to Studies on Ultrafast Protein Dynamics. *Bull. Chem. Soc. Jpn.* **2017**, *90*, 1344−1371.
(71) Kondoh, M.; Mizuno, M.; Mizutani, Y. Importance of Atomic Contacts in Vibrational Energy Flow in Proteins. *J. Phys. Chem. Lett.* **2016**, *7*, 1950−1954.
(72) Yu, X.; Leitner, D. M. Vibrational Energy Transfer and Heat Conduction in a Protein. *J. Phys. Chem. B* **2003**, *107*, 1698−1707.
(73) Nishikawa, T.; Go, N. Normal Modes of Vibration in Bovine Pancreatic Trypsin Inhibitor and Its Mechanical Property. *Proteins: Struct., Funct., Genet.* **1987**, *2*, 308−329.
(74) Schade, M.; Moretto, A.; Donaldson, P. M.; Toniolo, C.; Hamm, P. Vibrational Energy Transport through a Capping Layer of Appropriately Designed Peptide Helices over Gold Nanoparticles. *Nano Lett.* **2010**, *10*, 3057−3061.
(75) Schade, M.; Hamm, P. Transition from Ivr Limited Vibrational Energy Transport to Bulk Heat Transport. *Chem. Phys.* **2012**, *393*, 46−50.
(76) Schade, M.; Hamm, P. Vibrational Energy Transport in the Presence of Intrasite Vibrational Energy Redistribution. *J. Chem. Phys.* **2009**, *131*, No. 044511.
(77) Backus, E. H. G.; Nguyen, P. H.; Botan, V.; Pfister, R.; Moretto, A.; Crisma, M.; Toniolo, C.; Stock, G.; Hamm, P. Energy Transport in Peptide Helices: A Comparison between High- and Low-Energy Excitations. *J. Phys. Chem. B* **2008**, *112*, 9091−9099.
(78) Backus, E. H.; Bloem, R.; Pfister, R.; Moretto, A.; Crisma, M.; Toniolo, C.; Hamm, P. Dynamical Transition in a Small Helical Peptide and Its Implication for Vibrational Energy Transport. *J. Phys. Chem. B* **2009**, *113*, 13405−13409.

DOI: 10.1021/acs.jpcb.9b07086
J. Phys. Chem. B 2019, 123, 9507−9524

(79) Xu, Y.; Leitner, D. M. Vibrational Energy Flow through the Green Fluorescent Protein-Water Interface: Communication Maps and Thermal Boundary Conductance. *J. Phys. Chem. B* **2014**, *118*, 7818−7826.
(80) Leitner, D. M. Thermal Boundary Conductance and Thermal Rectification in Molecules. *J. Phys. Chem. B* **2013**, *117*, 12820−12828.
(81) Lervik, A.; Bresme, F.; Kjelstrup, S.; Bedeaux, D.; Rubi, J. M. Heat Transfer in Protein-Water Interfaces. *Phys. Chem. Chem. Phys.* **2010**, *12*, 1610−1617.
(82) Pandey, H. D.; Leitner, D. M. Small Saccharides as a Blanket around Proteins: A Computational Study. *J. Phys. Chem. B* **2018**, *122*, 7277−7285.
(83) Takei, Y.; Arai, S.; Murata, A.; Takabayashi, M.; Oyama, K.; Ishiwata, S.'i.; Takeoka, S.; Suzuki, M. A Nanoparticle-Based Ratiometric and Self-Calibrated Fluorescent Thermometer for Single Living Cells. *ACS Nano* **2014**, *8*, 198−206.
(84) Alicki, R.; Leitner, D. M. Size-Dependent Accuracy of Nanoscale Thermometers. *J. Phys. Chem. B* **2015**, *119*, 9000−9005.
(85) Baffou, G.; Rigneault, H.; Marguet, D.; Jullien, L. A Critique of Methods for Temperature Imaging in Single Cells. *Nat. Methods* **2014**, *11*, 899−901.
(86) Reid, K. M.; Pandey, H. D.; Leitner, D. M. Elastic and Inelastic Contributions to Thermal Transport between Chemical Groups and Thermal Rectification in Molecules. *J. Phys. Chem. C* **2019**, *123*, 6256−6264.
(87) Pandey, H. D.; Leitner, D. M. Influence of Thermalization on Thermal Conduction through Molecular Junctions: Computational Study of Peg Oligomers. *J. Chem. Phys.* **2017**, *147*, 084701.
(88) Pandey, H. D.; Leitner, D. M. Thermalization and Thermal Transport in Molecules. *J. Phys. Chem. Lett.* **2016**, *7*, 5062−5067.
(89) Leitner, D. M. Energy Relaxation and Thermal Transport in Molecules. In *Handbook of Materials Modeling*; Andreoni, W., Yip, S., Eds.; Springer: Cham, Switzerland, 2018.
(90) Bigwood, R.; Gruebele, M.; Leitner, D. M.; Wolynes, P. G. The Vibrational Energy Flow Transition in Organic Molecules: Theory Meets Experiment. *Proc. Natl. Acad. Sci. U. S. A.* **1998**, *95*, 5960−5964.
(91) Leitner, D. M. Influence of Quantum Energy Flow and Localization on Molecular Isomerization in Gas and Condensed Phases. *Int. J. Quantum Chem.* **1999**, *75*, 523−531.
(92) Leitner, D. M. Quantum Ergodicity and Energy Flow in Molecules. *Adv. Phys.* **2015**, *64*, 445−517.
(93) Leitner, D. M. Molecules and the Eigenstate Thermalization Hypothesis. *Entropy* **2018**, *20*, 673.
(94) Leitner, D. M.; Gruebele, M. A Quantum Model of Restricted Vibrational Energy Flow on the Way to the Transition State in Unimolecular Reactions. *Mol. Phys.* **2008**, *106*, 433−442.
(95) Leitner, D. M.; Wolynes, P. G. Statistical Properties of Localized Vibrational Eigenstates. *Chem. Phys. Lett.* **1996**, *258*, 18−24.
(96) Gruebele, M. Molecular Vibrational Energy Flow: A State Space Approach. *Adv. Chem. Phys.* **2007**, *114*, 193−261.
(97) Keshavamurthy, S. Scaling Perspective on Intramolecular Vibrational Energy Flow: Analogies, Insights and Challenges. *Adv. Chem. Phys.* **2013**, *153*, 43−110.
(98) Logan, D. E.; Wolynes, P. G. Quantum Localization and Energy Flow in Many-Dimensional Fermi Resonant Systems. *J. Chem. Phys.* **1990**, *93*, 4994−5012.
(99) Leitner, D. M.; Wolynes, P. G. Quantum Energy Flow During Molecular Isomerization. *Chem. Phys. Lett.* **1997**, *280*, 411−418.
(100) Leitner, D. M.; Levine, B.; Quenneville, J.; Martínez, T. J.; Wolynes, P. G. Quantum Energy Flow and Trans-Stilbene Photoisomerization: An Example of a Non-Rrkm Reaction. *J. Phys. Chem. A* **2003**, *107*, 10706−10716.
(101) Viitala, L.; Pajari, S.; Lajunen, T.; Kontturi, L.-S.; Laaksonen, T.; Kuomanen, P.; Viitala, T.; Urtti, A.; Murtomäki, L. Photothermally Triggered Lipid Bilayer Phase Transition and Drug Release from Gold Nanorod and Indocyanine Green Encapsulated Liposomes. *Langmuir* **2016**, *32*, 4554−4563.
(102) Qin, Z.; Bischof, J. C. Thermophysical and Biological Responses of Gold Nanoparticle Laser Heating. *Chem. Soc. Rev.* **2012**, *41*, 1191−1217.
(103) Hassan, S.; Schade, M.; Shaw, C. P.; Levy, P.; Hamm, P. Response of Villin Headpiece-Capped Gold Nanoparticles to Ultrafast Laser Heating. *J. Phys. Chem. B* **2014**, *118*, 7954−7962.
(104) Dreaden, E. C.; Austin, L. A.; Mackey, M. A.; El-Sayed, M. A. Size Matters: Gold Nanoparticles in Targeted Cancer Drug Delivery. *Ther. Delivery* **2012**, *3*, 457−478.
(105) Kauzmann, W.; Moore, K.; Schultz, D. Protein Densities from X-Ray Crystallographic Coordinates. *Nature* **1974**, *248*, 447−449.
(106) Knapp, J. E.; Pahl, R.; Srajer, V.; Royer, W. E. Allosteric Action in Real Time: Time-Resolved Crystallographic Studies of a Cooperative Dimeric Hemoglobin. *Proc. Natl. Acad. Sci. U. S. A.* **2006**, *103*, 7649−7654.
(107) Ren, Z.; Srajer, V.; Knapp, J. E.; Royer, W. E. Cooperative Macromolecular Device Revealed by Meta-Analysis of Static and Time-Resolved Structures. *Proc. Natl. Acad. Sci. U. S. A.* **2012**, *109*, 107−112.
(108) Achoch, M.; Dorantes-Gilardi, R.; Wymant, C.; Feverati, G.; Salamatian, K.; Vuillon, L.; Lesieur, C. Protein Structural Robustness to Mutations: An in Silico Investigation. *Phys. Chem. Chem. Phys.* **2016**, *18*, 13770−13780.
(109) Vuillon, L.; Lesieur, C. From Local to Global Changes in Proteins: A Network View. *Curr. Opin. Struct. Biol.* **2015**, *31*, 1−8.
(110) Ribeiro, A. A. S. T.; Ortiz, V. Energy Propagation and Network Energetic Coupling in Proteins. *J. Phys. Chem. B* **2015**, *119*, 1835−1846.
(111) Ribeiro, A. A. S. T.; Ortiz, V. Determination of Signaling Pathways in Proteins through Network Theory: Importance of the Topology. *J. Chem. Theory Comput.* **2014**, *10*, 1762−1769.
(112) Khor, S. Protein Residue Networks from a Local Search Perspective. *J. Complex Networks* **2016**, *4*, 245−278.
(113) Sethi, A.; Eargle, J.; Black, A. A.; Luthey-Schulten, Z. Dynamical Networks in Trna:Protein Complexes. *Proc. Natl. Acad. Sci. U. S. A.* **2009**, *106*, 6620−6625.
(114) Miao, Y.; Nichols, S. E.; Gasper, P. M.; Metzger, V. T.; McCammon, J. A. Activation and Dynamic Network of the M2Muscarinic Receptor. *Proc. Natl. Acad. Sci. U. S. A.* **2013**, *110*, 10982−10987.
(115) Livi, L.; Maiorino, E.; Giuliani, A.; Rizzi, A.; Sadeghian, A. A Generative Model for Protein Contact Networks. *J. Biomol. Struct. Dyn.* **2016**, *34*, 1441−1454.
(116) Karain, W. I.; Qaraeen, N. I. Weighted Protein Residue Networks Based on Joint Recurrences between Residues. *BMC Bioinf.* **2015**, *16*, 173.
(117) Gerek, Z. N.; Ozkan, S. B. Change in Allosteric Network Affects Binding Affinities of PDZ Domains: Analysis through Perturbation Response Scanning. *PLoS Comput. Biol.* **2011**, *7*, e1002154.
(118) Dokholyan, N. V. Controlling Allosteric Networks in Proteins. *Chem. Rev.* **2016**, *116*, 6463−6487.
(119) DiPaola, L.; DeRuvo, M.; Paci, P.; Santoni, D.; Giuliani, A. Protein Contact Networks: An Emerging Paradigm in Chemistry. *Chem. Rev.* **2013**, *113*, 1598−1613.
(120) Cyphers, S.; Ruff, E. F.; Behr, J. M.; Chodera, J. D.; Levinson, N. M. A Water-Mediated Allosteric Network Governs Activation of Aurora Kinase A. *Nat. Chem. Biol.* **2017**, *13*, 402−408.
(121) Csizmok, V.; Follis, A. V.; Kriwacki, R. W.; Forman-Kay, J. D. Dynamic Protein Interaction Networks and New Structural Paradigms in Signaling. *Chem. Rev.* **2016**, *116*, 6424−6462.
(122) Amor, B. R. C.; Schaub, M. T.; Yaliriki, S. N.; Barahona, M. Prediction of Allosteric Sites and Mediating Interactions through Bond-to-Bond Propensities. *Nat. Commun.* **2016**, *7*, 12477.
(123) Moritsugu, K.; Miyashita, O.; Kidera, A. Temperature Dependence of Vibrational Energy Transfer in a Protein Molecule. *J. Phys. Chem. B* **2003**, *107*, 3309−3317.
(124) Moritsugu, K.; Miyashita, O.; Kidera, A. Vibrational Energy Transfer in a Protein Molecule. *Phys. Rev. Lett.* **2000**, *85*, 3970−3973.

DOI: 10.1021/acs.jpcb.9b07086
J. Phys. Chem. B 2019, 123, 9507−9524

(125) Xu, Y.; Leitner, D. M. Communication Maps of Vibrational Energy Transport in Photoactive Yellow Protein. *J. Phys. Chem. A* **2014**, *118*, 7280−7287.
(126) Yu, X.; Leitner, D. M. Heat Flow in Proteins: Computation of Thermal Transport Coefficients. *J. Chem. Phys.* **2005**, *122*, 054902.
(127) Leitner, D. M. Heat Transport in Molecules and Reaction Kinetics: The Role of Quantum Energy Flow and Localization. *Adv. Chem. Phys.* **2005**, *130B*, 205−256.
(128) Foley, B. M.; Gorham, C. S.; Duda, J. C.; Cheaito, R.; Szwejkowski, C. J.; Constantin, C.; Kaehr, B.; Hopkins, P. E. Protein Thermal Conductivity Measured in the Solid State Reveals Anharmonic Interactions of Vibrations in a Fractal Structure. *J. Phys. Chem. Lett.* **2014**, *5*, 1077−1082.
(129) Leitner, D. M. Heat Transport in Proteins. In *Proteins: Energy, Heat and Signal Flow*; Leitner, D. M., Straub, J. E., Eds.; Taylor and Francis: New York, 2010; pp 247−270.
(130) Heyden, M.; Tobias, D. J. Spatial Dependence of Protein-Water Collective Hydrogen Bond Dynamics. *Phys. Rev. Lett.* **2013**, *111*, No. 218101.
(131) Ebbinghaus, S.; Kim, S.-J.; Heyden, M.; Yu, X.; Heugen, U.; Gruebele, M.; Leitner, D. M.; Havenith, M. An Extended Dynamical Solvation Shell around Proteins. *Proc. Natl. Acad. Sci. U. S. A.* **2007**, *104*, 20749−20752.
(132) Luong, T. Q.; Xu, Y.; Bründermann, E.; Leitner, D. M.; Havenith, M. Hydrophobic Collapse Induces Changes in the Collective Protein and Hydration Low Frequency Modes. *Chem. Phys. Lett.* **2016**, *651*, 1−7.
(133) Meister, K.; Ebbinghaus, S.; Xu, Y.; Duman, J. G.; DeVries, A.; Gruebele, M.; Leitner, D. M.; Havenith, M. Long-Range Protein-Water Dynamics in Hyperactive Insect Antifreeze Proteins. *Proc. Natl. Acad. Sci. U. S. A.* **2013**, *110*, 1617−22.
(134) Xu, Y.; Havenith, M. Perspective: Watching Low-Frequency Vibrations of Water in Biomolecules by Thz Spectroscopy. *J. Chem. Phys.* **2015**, *143*, 170901.
(135) Wirtz, H.; Schäfer, S.; Hoberg, C.; Reid, K. M.; Leitner, D. M.; Havenith, M. Hydrophobic Collapse of Ubiquitin Generates Rapid Protein-Water Motions. *Biochemistry* **2018**, *57*, 3650−3657.
(136) Pandey, H. D.; Leitner, D. M. Thermodynamics of Hydration Water around an Antifreeze Protein: A Molecular Simulation Study. *J. Phys. Chem. B* **2017**, *121*, 9498−9507.
(137) Yu, X.; Park, J.; Leitner, D. M. Thermodynamics of Protein Hydration Computed by Molecular Dynamics and Normal Modes. *J. Phys. Chem. B* **2003**, *107*, 12820−12829.
(138) Frauenfelder, H.; Fenimore, P. W.; Chan, G.; McMahon, B. H. Protein Folding Is Slaved to Solvent Motions. *Proc. Natl. Acad. Sci. U. S. A.* **2006**, *103*, 15469−15472.
(139) Buchli, B.; Waldauer, S. A.; Walser, R.; Donten, M. L.; Pfister, R.; Blöchliger, N.; Steiner, S.; Caflisch, A.; Zerbe, O.; Hamm, P. Kinetic Response of a Photoperturbed Allosteric Protein. *Proc. Natl. Acad. Sci. U. S. A.* **2013**, *110*, 11725−11730.
(140) Park, S.-M.; Nguyen, P. H.; Stock, G. Molecular Dynamics Simulation of Cooling: Heat Transfer from a Photoexcited Peptide to the Solvent. *J. Chem. Phys.* **2009**, *131*, 184503.
(141) Nguyen, P. H.; Park, S. M.; Stock, G. Nonequilibrium Molecular Dynamics Simulation of the Energy Transfer through a Peptide Helix. *J. Chem. Phys.* **2010**, *132*, 025102.
(142) Backus, E. H. G.; Nguyen, P. H.; Botan, V.; Moretto, A.; Crisma, M.; Toniolo, C.; Zerbe, O.; Stock, G.; Hamm, P. Structural Flexibility of a Helical Peptide Regulates Vibrational Energy Transport Properties. *J. Phys. Chem. B* **2008**, *112*, 15487−15492.
(143) Atilgan, A. R.; Durell, S. R.; Jernigan, R. L.; Demirel, M. C.; Keskin, O.; Bahar, I. Anisotropy of Fluctuation Dynamics of Proteins with an Elastic Network Model. *Biophys. J.* **2001**, *80*, 505−515.
(144) Miyashita, O.; Wolynes, P. G.; Onuchic, J. N. Simple Energy Landscape Model for the Kinetics of Functional Transitions in Proteins. *J. Phys. Chem. B* **2005**, *109*, 1959−1969.
(145) Miyashita, O.; Onuchic, J. N.; Wolynes, P. G. Nonlinear Elasticity, Protein-Quakes, and the Energy Landscape of Functional Transitions in Proteins. *Proc. Natl. Acad. Sci. U. S. A.* **2003**, *100*, 12570−12575.
(146) Nakayama, T.; Kousuke, Y.; Orbach, R. L. Dynamical Properties of Fractal Networks: Scaling, Numerical Simulations, and Physical Realizations. *Rev. Mod. Phys.* **1994**, *66*, 381−443.
(147) Alexander, S.; Orbach, R. Density of States of Fractals: 'Fractons'. *J. Phys., Lett.* **1982**, *43*, 625−631.
(148) Alexander, S.; Bernasconi, J.; Scheider, W. R.; Orbach, R. Excitation Dynamics in Random One-Dimensional Systems. *Rev. Mod. Phys.* **1981**, *53*, 175−198.
(149) Rammal, R.; Toulouse, G. Random Walks on Fractal Structures and Percolation Clusters. *J. Phys., Lett.* **1983**, *44*, 13−22.
(150) Ishikura, T.; Iwata, Y.; Hatano, T.; Yamato, T. Energy Exchange Network of Inter-Residue Interactions within a Thermally Fluctuating Protein: A Computational Study. *J. Comput. Chem.* **2015**, *36*, 1709−1718.
(151) Yamato, T. Energy Flow Pathways in Photoreceptor Proteins. In *Proteins: Energy, Heat and Signal Flow*, Leitner, D. M., Straub, J. E., Eds.; CRC Press, Taylor and Francis Group: Boca Raton, FL, 2010; pp 129−147.
(152) Wand, A. J.; Sharp, K. A. Measuring Entropy in Molecular Recognition by Proteins. *Annu. Rev. Biophys.* **2018**, *47*, 41−61.
(153) Wand, A. J. The Dark Energy of Proteins Comes to Light: Conformational Entropy and Its Role in Protein Function Revealed by Nmr Relaxation. *Curr. Opin. Struct. Biol.* **2013**, *23*, 75−81.
(154) Tzeng, S.-R.; Kalodimos, C. G. Protein Activity Regulation by Conformational Entropy. *Nature* **2012**, *488*, 236−240.
(155) Kasinath, V.; Sharp, K. A.; Wand, A. J. Microscopic Insights into the Nmr Relaxation-Based Protein Conformational Entropy Meter. *J. Am. Chem. Soc.* **2013**, *135*, 15092−15100.
(156) Frederick, K. K.; Marlow, M. S.; Valentine, K. G.; Wand, A. J. Conformational Entropy in Molecular Recognition by Proteins. *Nature* **2007**, *448*, 325−329.
(157) Caro, J. A.; Harpole, K. W.; Kasinath, V.; Lim, J.; Granja, J.; Valentine, K. G.; Sharp, K. A.; Wand, A. J. Entropy in Molecular Recognition by Proteins. *Proc. Natl. Acad. Sci. U. S. A.* **2017**, *114*, 6563−6568.
(158) Lervik, A.; Bresme, F.; Kjelstrup, S. Heat Transfer in Soft Nanoscale Interfaces: The Influence of Interface Curvature. *Soft Matter* **2009**, *5*, 2407−2414.
(159) Li, P.; Champion, P. M. Investigations of the Thermal Response of Laser-Excited Biomolecules. *Biophys. J.* **1994**, *66*, 430−436.
(160) Mancini, R. J.; Lee, J.; Maynard, H. D. Trehalose Glycopolymers for Stabilization of Protein Conjugates to Environmental Stressors. *J. Am. Chem. Soc.* **2012**, *134*, 8474−8479.
(161) Kaushik, J. K.; Bhat, R. Why Is Trehalose an Exceptional Protein Stabilizer? *J. Biol. Chem.* **2003**, *278*, 26458−26465.
(162) Yu, X.; Leitner, D. M. Thermal Transport Coefficients for Liquid and Glassy Water Computer from a Harmonic Aqueous Glass. *J. Chem. Phys.* **2005**, *123*, 104503.
(163) Acharya, H.; Mozdzierz, N. J.; Keblinski, P.; Garde, S. How Chemistry, Nanoscale Roughness, and the Direction of Heat Flow Affect Thermal Conductance of Solid-Water Interfaces. *Ind. Eng. Chem. Res.* **2012**, *51*, 1767−1773.
(164) Heugen, U.; Schwaab, G.; Bründermann, E.; Heyden, M.; Yu, X.; Leitner, D. M.; Havenith, M. Solute Induced Retardation of Water Dynamics: Hydration Water Probed Directly by Thz Spectroscopy. *Proc. Natl. Acad. Sci. U. S. A.* **2006**, *103*, 12301−12306.
(165) Heyden, M.; Bründermann, E.; Heugen, U.; Niehues, G.; Leitner, D. M.; Havenith, M. The Long Range Influence of Carbohydrates on the Solvation Dynamics of Water − Answers from Thz Spectroscopic Measurements and Molecular Modelling Simulations. *J. Am. Chem. Soc.* **2008**, *130*, 5773−5779.
(166) Stocker, K. M.; Neidhart, S. M.; Gezelter, J. D. Interfacial Thermal Conductance of Thiolate-Protected Gold Nanospheres. *J. Appl. Phys.* **2016**, *119*, 025106.
(167) Neidhart, S. M.; Gezelter, J. D. Thermal Transport Is Influenced by Nanoparticle Morphology: A Molecular Dynamics Study. *J. Phys. Chem. C* **2018**, *122*, 1430−1436.

DOI: 10.1021/acs.jpcb.9b07086
J. Phys. Chem. B 2019, 123, 9507−9524

(168) Kuang, S.; Gezelter, J. D. Simulating Interfacial Thermal Conductance at Metal-Solvent Interfaces: The Role of Chemical Capping Agents. *J. Phys. Chem. C* **2011**, *115*, 22475−22483.
(169) Stocker, K. M.; Gezelter, J. D. Simulations of Heat Conduction at Thiolate-Capped Gold Surfaces: The Role of Chain Length and Solvent Penetration. *J. Phys. Chem. C* **2013**, *117*, 7605−7612.
(170) Zhang, T.; Luo, T. Giant Thermal Rectification from Polyethylene Nanofiber Thermal Diodes. *Small* **2015**, *11*, 4657−4665.
(171) Wu, X.; Varshney, V.; Lee, J.; Pang, Y.; Roy, A. K.; Luo, T. How to Characterize Thermal Transport Capability of 2d Materials Fairly? − Sheet Thermal Conductance and the Choice of Thickness. *Chem. Phys. Lett.* **2017**, *669*, 233−237.
(172) Majumdar, S.; Malen, J. A.; McGaughey, A. J. H. Cooperative Molecular Behavior Enhances the Thermal Conductance of Binary Self-Assembled Monolayer Junctions. *Nano Lett.* **2017**, *17*, 220−227.
(173) Gaskins, J. T.; Bulusu, A.; Giordano, A. J.; Duda, J. C.; Graham, S.; Hopkins, P. E. Thermal Conductance across Phosphonic Acid Molecules and Interfaces: Ballistic Versus Diffusive Vibrational Transport in Molecular Monolayers. *J. Phys. Chem. C* **2015**, *119*, 20931−20939.
(174) Majumdar, S.; Sierra-Suarez, J. A.; Schiffres, S. N.; Ong, W.-L.; Higgs, C. F.; McGaughey, A. J. H.; Malen, J. A. Vibrational Mismatch of Metal Leads Controls Thermal Conductance of Self-Assembled Monolayer Junctions. *Nano Lett.* **2015**, *15*, 2985−2991.
(175) Galperin, M.; Nitzan, A.; Ratner, M. A. Heat Conduction in Molecular Transport Junctions. *Phys. Rev. B: Condens. Matter Mater. Phys.* **2007**, *75*, 155312.
(176) Segal, D.; Nitzan, A.; Hänggi, P. Thermal Conductance through Molecular Wires. *J. Chem. Phys.* **2003**, *119*, 6840−6855.
(177) Buldum, A.; Leitner, D. M.; Ciraci, S. Thermal Conduction through a Molecule. *Europhys. Lett.* **1999**, *47*, 208−212.
(178) Cui, L.; Miao, R.; Jiang, C.; Meyhofer, E.; Reddy, P. Perspective: Thermal and Thermoelectric Transport in Molecular Junctions. *J. Chem. Phys.* **2017**, *146*, 092201.
(179) Segal, D.; Agarwalla, B. K. Vibrational Heat Transport in Molecular Junctions. *Annu. Rev. Phys. Chem.* **2016**, *67*, 185−209.
(180) Moghaddasi Fereidani, R.; Segal, D. Phononic Heat Transport in Molecular Junctions: Quantum Effects and Vibrational Mismatch. *J. Chem. Phys.* **2019**, *150*, 024105.
(181) Li, Q.; Strange, M.; Duchemin, I.; Donadio, D.; Solomon, G. C. A Strategy to Suppress Phonon Transport in Molecular Junctions Using Π-Stacked Systems. *J. Phys. Chem. C* **2017**, *121*, 7175−7182.
(182) Li, Q.; Duchemin, I.; Xiong, S.; Solomon, G. C.; Donadio, D. Mechanical Tuning of Thermal Transport in a Molecular Junction. *J. Phys. Chem. C* **2015**, *119*, 24636−24642.
(183) Eustis, S.; El-Sayed, M. A. Why Gold Nanoparticles Are More Precious Than Pretty Gold: Noble Metal Surface Plasmon Resonance and Its Enhancement of the Radiative and Nonradiative Properties of Nanocrystals of Different Shapes. *Chem. Soc. Rev.* **2006**, *35*, 209−217.
(184) Sahoo, D.; Bhattacharya, P.; Patra, H. K.; Mandal, P.; Chakravorti, S. Gold Nanoparticle Induced Conformational Changes in Heme Protein. *J. Nanopart. Res.* **2011**, *13*, 6755−6760.
(185) Losego, M. D.; Grady, M. E.; Sottow, N. R.; Cahill, D. G.; Braun, P. V. Effects of Chemical Bonding on Heat Transport across Interfaces. *Nat. Mater.* **2012**, *11*, 502−506.
(186) Giri, A.; Niemela, J.-P.; Tynell, T.; Gaskins, J. T.; Donovan, B. F.; Karppinen, M.; Hopkins, P. E. Heat-Transport Mechanisms in Molecular Building Blocks of Inorganic/Organic Hybrid Superlattices. *Phys. Rev. B: Condens. Matter Mater. Phys.* **2016**, *93*, 115310.
(187) Tomko, J. A.; Pena-Francesch, A.; Jung, H.; Tyagi, M.; Allen, B. D.; Demirel, M. C.; Hopkins, P. E. Tunable Thermal Transport and Reversible Thermal Conductivity Switching in Topologically Networked Bio-Inspired Materials. *Nat. Nanotechnol.* **2018**, *13*, 959−964.
(188) Yue, Y.; Qasim, L. N.; Kurnosov, A. A.; Rubtsova, N. I.; Mackin, R. T.; Zhang, H.; Zhang, B. Y.; Zhou, X.; Jayawickramarajah, J.; Burin, A. L.; et al. Band-Selective Ballistic Energy Transport in Alkane Oligomers: Toward Controlling the Transport Speed. *J. Phys. Chem. B* **2015**, *119*, 6448−6456.
(189) Rubtsova, N. I.; Qasim, L. N.; Kurnosov, A. A.; Burin, A. L.; Rubtsov, I. V. Ballistic Energy Transport in Oligomers. *Acc. Chem. Res.* **2015**, *48*, 2547−2555.
(190) Qasim, L. N.; Atuk, E. B.; Maksymov, A. O.; Jayawickramarajah, J.; Burin, A. L.; Rubtsov, I. V. Ballistic Transport of Vibrational Energy through an Amide Group Bridging Alkyl Chains. *J. Phys. Chem. C* **2019**, *123*, 3381−3392.
(191) Rubtsov, I. V.; Burin, A. L. Ballistic and Diffusive Vibrational Energy Transport in Molecules. *J. Chem. Phys.* **2019**, *150*, 020901.
(192) Pandey, H. D.; Leitner, D. M. Vibrational Energy Transport in Molecules and the Statistical Properties of Vibrational Modes. *Chem. Phys.* **2017**, *482*, 81−85.
(193) Cui, L.; Hur, S.; Zkbar, Z. A.; Klöckner, J. C.; Jeong, W.; Pauly, F.; Jang, S.-Y.; Reddy, P.; Meyhofer, E. Thermal Conductance of Single-Molecule Junctions. *Nature* **2019**, *572*, 628−633.
(194) Meier, T.; Menges, F.; Nirmalraj, P.; Hölscher, H.; Riel, H.; Gotsmann, B. Length-Dependent Thermal Transport Along Molecular Chains. *Phys. Rev. Lett.* **2014**, *113*, 060801.
(195) Craven, G. T.; Nitzan, A. Electron Transfer at Thermally Heterogeneous Molecule-Metal Interfaces. *J. Chem. Phys.* **2017**, *146*, 092305.
(196) Craven, G. T.; Nitzan, A. Electron Transfer across a Thermal Gradient. *Proc. Natl. Acad. Sci. U. S. A.* **2016**, *113*, 9421−9429.
(197) Chen, R.; Craven, G. T.; Nitzan, A. Electron-Transfer-Induced and Phononic Heat Transport in Molecular Environments. *J. Chem. Phys.* **2017**, *147*, 124101.
(198) Pein, B. C.; Sun, Y.; Dlott, D. D. Controlling Vibrational Energy Flow in Liquid Alkylbenzenes. *J. Phys. Chem. B* **2013**, *117*, 10898−10904.
(199) Pein, B. C.; Sun, Y.; Dlott, D. D. Unidirectional Vibrational Energy Flow in Nitrobenzene. *J. Phys. Chem. A* **2013**, *117*, 6066−6072.
(200) Pein, B. C.; Dlott, D. D. Modifying Vibrational Energy Flow in Aromatic Molecules: Effects of Ortho Substitution. *J. Phys. Chem. A* **2014**, *118*, 965−973.
(201) Leitner, D. M.; Pandey, H. D. Quantum Bottlenecks and Unidirectional Energy Flow in Molecules. *Ann. Phys.* **2015**, *527*, 601−609.
(202) Leitner, D. M.; Pandey, H. D. Asymmetric Energy Flow in Liquid Alkylbenzenes: A Computational Study. *J. Chem. Phys.* **2015**, *143*, 144301.
(203) Segal, D.; Nitzan, A. Heat Rectification in Molecular Junctions. *J. Chem. Phys.* **2005**, *122*, 194704.
(204) Wu, L.-A.; Segal, D. Sufficient Conditions for Thermal Rectification in Hybrid Quantum Structures. *Phys. Rev. Lett.* **2009**, *102*, No. 095503.
(205) Miño-Galaz, G. A.; Gutierrez, G. Hydrogen Bonds and Asymmetrical Heat Diffusion in A-Helices. A Computational Analysis. *Chem. Phys. Lett.* **2015**, *635*, 16−22.
(206) Miño-Galaz, G. A. Allosteric Communication Pathways and Thermal Rectification in PDZ2 Protein: A Computational Study. *J. Phys. Chem. B* **2015**, *119*, 6179−6189.
(207) Kukura, P.; McCamant, D. W.; Yoon, S.; Wandschneider, D. B.; Mathies, R. A. Structural Observation of the Primary Isomerization in Vision with Femtosecond-Stimulated Raman. *Science* **2005**, *310*, 1006−1009.
(208) Kim, J. E.; Tauber, M. J.; Mathies, R. A. Analysis of the Mode-Specific Excited-State Energy Distribution and Wavelength-Dependent Photoreaction Quantum Yield in Rhodopsin. *Biophys. J.* **2003**, *84*, 2492−2501.
(209) Leitner, D. M. Quantum Localization and Protein-Assisted Vibrational Energy Flow in Cofactors. *New J. Phys.* **2010**, *12*, 085004.
(210) Leitner, D. M. Mode Damping Rates in a Protein Chromophore. *Chem. Phys. Lett.* **2012**, *530*, 102−106.
(211) Lee, Y.; Choi, S.; Hyeon, C. Mapping the Intramolecular Signal Tranduction of G-Protein Coupled Receptors. *Proteins: Struct., Funct., Genet.* **2014**, *82*, 727−743.
(212) Thirumalai, D.; Hyeon, C. Signalling Networks and Dynamics of Allosteric Transitions in Bacterial Chaperonin Groel: Implications

DOI: 10.1021/acs.jpcb.9b07086
J. Phys. Chem. B 2019, 123, 9507−9524

for Iterative Annealing of Misfolded Proteins. *Philos. Trans. R. Soc., B* **2018**, *373*, 20170182.
(213) Hyeon, C.; Onuchic, J. N. Energy Balance and Dynamics of Kinesin Motors. In *Proteins: Energy, Heat and Signal Flow*; Leitner, D. M., Straub, J. E., Eds.; CRC Press, Taylor & Frances Group: Boca Raton, FL, 2010; pp 3−21.
(214) Lu, C.; Knecht, V.; Stock, G. Long-Range Conformational Response of a PDZ Domain to Ligand Binding and Release: A Molecular Dynamics Study. *J. Chem. Theory Comput.* **2016**, *12*, 870−878.

DOI: 10.1021/acs.jpcb.9b07086
J. Phys. Chem. B 2019, 123, 9507−9524